Numb/Numbl-Opo antagonism controls retinal epithelium morphogenesis by regulating integrin endocytosis

Bogdanović Ozren[1]*, Delfino-Machín Mariana[1]*, Nicolás-Pérez María[1], Gavilán María P.[2], Gago-Rodrigues Inês[1], Fernández-Miñán Ana[1], Lillo Concepción[3], Ríos Rosa M.[2], Wittbrodt Joachim[4], Martínez-Morales Juan R.[1#]*

1. Centro Andaluz de Biología del Desarrollo (CSIC/UPO/JA), 41013 Sevilla, Spain

2. CABIMER (CSIC), 41092 Sevilla, Spain

3. INCYL (University of Salamanca), 37007 Salamanca, Spain

4. COS, Heidelberg University and ITG, Karslruhe Institute of Technology, Germany

*Equal contribution

[#]Correspondence: jrmarmor@upo.es

Phone: +34954977827

Running Title: *Numbs/Opo antagonism controls optic cup formation*

Summary

Polarized trafficking of adhesion receptors plays a pivotal role in controlling cellular behavior during morphogenesis. Particularly, clathrin-dependent endocytosis of integrins has long been acknowledged as essential for cell migration. However, little is known on the contribution of integrin trafficking to epithelial tissue morphogenesis. Here we show how the transmembrane protein Opo, previously described for its essential role during optic cup folding, plays a fundamental role in this process. Through interaction with the PTB domain of the clathrin adaptors Numb and Numbl via an integrin-like NPxF motif, Opo antagonizes Numb/Numbl function and acts as a negative regulator of integrin endocytosis *in vivo*. Accordingly, *numb/numbl* gain-of-function experiments in teleost embryos mimic the retinal malformations observed in *opo* mutants. We propose that developmental regulator *Opo* enables polarized Integrins localization by modulating Numb/Numbl, thus directing the basal constriction that shapes the vertebrate retina epithelium.

Introduction

In each metazoan group, stereotyped morphogenetic movements shape embryonic tissues into functional organs. During development and tissue remodeling precursor cells display a number of characteristic behaviors: cells may move freely, migrate as coordinated clusters and chains, or collectively change their shape to force an epithelial sheet to elongate, protrude, bend or form a tube (Lecuit and Lenne, 2007; Montell, 2008). How cells move and change their shape in a coordinated fashion depends both on the genetic identity of individual cells and on their microenvironment, which conditions cell signaling and adhesion (Papusheva and Heisenberg, 2010). The cytoskeletal machineries that generate and transmit morphogenetic tensions are locally assembled to drive the asymmetric behavior of the cells. This phenomenon is tightly linked to the regulation of general cell polarity and polarized trafficking of receptors and adhesion molecules (Bryant and Mostov, 2008; Nelson, 2009).

During tissue morphogenesis, polarized epithelial sheets bend to form cups, tubes and cysts, thus providing an important resource for evolutionary plasticity. The best-characterized example amongst morphogenetic events in animal epithelia is apical constriction (Sawyer et al., 2010). Quantitative imaging studies in *Drosophila* epithelia have shown that this process is driven by the periodic contractions of the actomyosin network at the cell apex (Martin et al., 2009; Solon et al., 2009). In epithelial sheets, bending may also occur towards the basal surface and examples of this behavior are observed in vertebrates during the formation of the midbrain-hindbrain boundary and the folding of the optic cup (Gutzman et al., 2008; Martinez-Morales and Wittbrodt, 2009). Basal cell contraction has also been recently described as the driving force directing the elongation of both the egg chamber in *Drosophila* (He et al., 2010) and the notochord in ascidians (Dong et al., 2011). Together, these studies show that basal constrictions/contractions involve the local recruitment of the actomyosin network. Furthermore, oscillatory actomyosin contractions, similar to those described at the apical surface, have also been recorded at the basal cell surface (He et al., 2010). Although these observations point to common characteristics for the contractile machineries operating at both ends of the apico-basal axis, clear differences also exist. Whereas apical constriction depends on adherens junctions and apical polarity

complexes (Kolsch et al., 2007; Letizia et al., 2011), it is integrins within focal adhesions that play a pivotal role in basally driven morphogenetic processes. Thus, interference with the adhesive function of integrins impairs basal actomyosin recruitment and tissue morphogenesis in both vertebrate and invertebrate epithelia (He et al., 2010; Martinez-Morales et al., 2009).

The fundamental role of focal adhesions in tissue morphogenesis has been best characterized in the context of cell migration, where clathrin-dependent trafficking of integrins along the front-back axis has proven to be essential for directional cell movement (Ezratty et al., 2009). Members of the phosphotyrosine binding (PTB) family of clathrin adaptors (such as Numb, Dab2 and ARH) interact with integrin-β NPxY/F motifs to regulate their endocytosis rate (Calderwood et al., 2003). Accordingly, both Dab2 and Numb regulate integrin-β turnover and directional cell migration in HeLa cells (Nishimura and Kaibuchi, 2007; Teckchandani et al., 2009). Despite the increasing evidence showing that polarized integrin endocytosis is essential for cell polarity and migration (Caswell et al., 2009; Nelson, 2009), the role of PTB clathrin adaptors in tissue morphogenesis is just beginning to be understood. Besides its traditional role in asymmetric cell division (Knoblich et al., 1995), the endocytic adaptor protein Numb has also been implicated in the regulation of different cellular processes including cell adhesion and polarity (Rasin et al., 2007; Wang et al., 2009). Studies using double-knockout mice for *Numb* and *Numb-like (Numbl)* have shown *in vivo* the redundant role of *numb* family members during axonal arborization (Huang et al., 2005) spindle orientation (Wu et al., 2010) and chemotaxis (Zhou et al., 2011). In polarized epithelial cells Numb asymmetrically localizes to the basolateral cortex (Dho et al., 2006). Both in epithelial and migratory cells, as well as during asymmetric cell divisions, the polarized localization of Numb depends on its phosphorylation by aPKC (Smith et al., 2007). In the context of migratory cells this polarized distribution has been related to a role in integrin recycling and cell motility (Nishimura and Kaibuchi, 2007). In contrast, although the severe neural tube defects observed in *Numb*$^{-/-}$ mice suggest a role in epithelial morphogenesis (Zhong et al., 2000), the functional significance of Numb polarized localization in epithelial cells is still unclear.

We have previously described the essential role of the transmembrane protein Opo, encoded by the gene *ojoplano/Ofcc1*, during optic cup morphogenesis. Opo regulates the

asymmetric localization of focal adhesion components to the basal surface of the retina epithelium and consequently, *ojoplano* loss-of-function impairs basal constriction in the teleost retina (Martinez-Morales et al., 2009). To further investigate Opo function, we carried out a yeast two-hybrid screen that identified PTB clathrin adaptors as its interacting partners. Here, we show that Opo interacts with the PTB domain of the adaptors, Numb and Numbl, through a conserved NPxF motif located in the amino terminal end of the protein. Using internalization assays and functional studies in mammalian cells and fish embryos, we demonstrate that Opo and Numb/Numbl act antagonistically to regulate integrin-β trafficking and optic cup morphogenesis. Our data indicate that Opo acts as a negative regulator of integrin endocytosis at the basal surface of the retina. These findings highlight the key role of integrin recycling as a developmental mechanism driving basal constriction during epithelial morphogenesis.

Results

Opo interacts with the PTB domain of Numb/Numbl through a conserved NPxF motif

The morphogenetic gene *opo* encodes a transmembrane protein (Opo) that regulates the polarized localization of focal adhesions in the retinal epithelium through a still uncharacterized molecular mechanism (Martinez-Morales et al., 2009). Besides four putative transmembrane passes (Figure 1A), Opo does not include any annotated protein domains that could suggest its molecular role. To gain insight into Opo molecular function we decided to identify its interacting partners using a yeast-two hybrid approach. As baits, we used the conserved N-terminal (N-Opo) and C-terminal (C-Opo) regions of the protein, both of which face the cytosolic compartment as indicated by topology prediction and also confirmed by epitope tagging (Figure S1). After screening 74 and 64 million interactions respectively, two members of the PTB family of endocytic adaptors **(**Numbl and Dab2**)** were identified as the highest-scoring proteins for the N-terminal bait (Table S1A), whereas the strongest C-terminal interaction was confirmed as Hsc70/Hspa1l (Table S1B), a chaperone belonging to the Hsp70s family. Both the PTB family members as well as Hsc70 are known regulators of clathrin-mediated endocytosis (Chang et al., 2002; Teckchandani et al., 2009; Ungewickell and Hinrichsen, 2007).

Upon closer inspection of the N-Opo sequence, a conserved NPxF motif congruous with the NPxY motif present in integrin-β tails was discovered (Figure 1B). Biochemical interaction of PTB domain proteins and NPxY/F ligands has been well documented *in vivo* and *in vitro* (Calderwood et al., 2003; Chen et al., 2006). These observations prompted us to examine the possibility that the Opo NPxF signal might interact with the PTB domain containing proteins: Numb, Numbl and Dab2, in a similar fashion. To that end, the PTB-containing N-terminal domains of these proteins were recombinantly expressed in bacteria and purified (Figure 1C-D). Glutathione S-transferase (GST) pulldowns of radiolabelled full-length Opo confirmed the biochemical interaction of N-Dab2, N-Numb and N-Numbl with the Opo protein (Figure 1D). Similarly, all three tested PTB proteins interacted *in vitro*, albeit to different extents, with the Integrin-β1 tail bearing the canonical NPxY sequence (Figure 1D). The converse experiment was also performed, and the immobilized N-Opo was incubated with radiolabelled N-Dab2, N-Numb and N-Numbl or their corresponding

full-length proteins (Figure 1E). Whereas the interaction of N-Opo with N-Numb/N-Numbl was corroborated in this assay, neither N-Dab2 nor Dab2 were recovered after incubation with immobilized N-Opo, suggesting that additional protein domains might play a role in stabilizing this interaction. Moreover, to test the ability of Opo to interact with PTB domain proteins within a physiological context, either a mammalian Opo-GFP fusion or GFP protein alone control were co-expressed together with Myc-tagged N-Numbl (*pCS2+:Myc-N-Numbl*) in the immortalized retinal pigment epithelial cell line, RPE-1. Western blotting of cellular extracts immunoprecipitated with anti-GFP antibody resulted in a clear signal identified by anti-GFP and anti-Myc antibodies, thereby confirming the biochemical interaction of Opo and Numbl in a mammalian system (Figure 1F).

These findings are further supported by colocalization experiments performed in HeLa cells where the full length Opo-GFP fusion was co-expressed together with a Numb-Cherry fusion (*pCS2+:zNumb:Cherry*) and analyzed by confocal microscopy (Figure 1G). In spite of their differential routing within the cell, Opo is trafficked through the secretory pathway whereas Numb preferentially localizes to the cell cortex (Knoblich et al., 1995); both proteins overlapped locally at the plasma membrane (Figure 1G).

Finally, to test whether the NPxF sequence present in the Opo N-terminus is indeed responsible for the interaction with PTB domain proteins, a point mutagenesis approach was undertaken. It has been previously demonstrated that the tyrosine residue present in Integrin NPxY tail sequences is crucial for cell motility and interaction with clathrin adaptors (Chen et al., 2006; Filardo et al., 1995). The phenylalanine present in the Opo motif was therefore mutated to either tyrosine or aspartic acid yielding NPAY or NPAD, respectively. The substitution of phenylalanine to tyrosine led to a modest (~2 fold) reduction in PTB domain binding as assayed by GST pull-down, whereas the substitution to aspartate resulted in a severe (> 10 fold) loss of protein interactions (Figure 1H-I). Both N-Numb and N-Numbl binding were equally affected by the mutation. Altogether, these data provide evidence for the interaction of Opo with PTB domain proteins and demonstrate the requirement of the NPxF sequence in enabling these interactions.

Opo localizes to a subpopulation of clathrin-coated structures

Numb localizes to Ap2α-positive clathrin-coated structures (CCSs) in HeLa cells, preferentially at the adhesion surface (Nishimura and Kaibuchi, 2007; Santolini et al., 2000). To investigate whether Opo shows a similar distribution, we transfected both HeLa and RPE-1 cells with either N-terminal (GFP-Opo) or C-terminal (Opo-GFP) fusions (Figures 2 and S2) and examined their subcellular localization. In agreement with our previous observations, Opo localized to different compartments along the secretory pathway including the ER, Golgi and the plasma membrane, as determined by co-staining with BIP, GM130 and F-actin respectively (data not shown). Opo also co-localized with a subpopulation of Ap2α-positive CCSs both in RPE-1 and HeLa cells, preferentially at the cellular cortex (Figures 2B-D; S2).

To investigate the specificity of this colocalization, HeLa cells were transfected with either a carboxy-terminal truncation of the protein (Figure 2E-G) or with OpoB, a mouse protein isoform (Mertes et al 2009) naturally truncated at the amino terminus (Figure 2H-J). The truncation of both Opo N- and C-terminus resulted in a substantial reduction of its colocalization with Ap2α, suggesting that both protein ends are required for Opo recruitment to CCSs.

Opo inhibits integrin internalization in HeLa cells

Previous reports in HeLa cells have shown that Numb interacts with the cytoplasmic Integrin-β tails and functions in their endocytosis (Calderwood et al., 2003; Nishimura and Kaibuchi, 2007; Teckchandani et al., 2009). Here we demonstrate that Opo localizes to a subpopulation of endocytic vesicles and interacts physically with Numb and Numbl. These results suggest that Opo may act as a regulator of integrin endocytosis. To functionally address this point we carried out internalization assays in HeLa cells (Figure 3). Transfected cells expressing either control *GFP*, *Opo-eGFP*, or *Numb-Cherry* were incubated with anti-Integrin-β1 antibodies for 30 or 40 minutes to allow its internalization. Cells were then fixed and the relative rate of Integrin endocytosis was calculated as the ratio between neighbor-transfected and non-transfected cells (expressed as %). As expected from the reported role for Numb in endocytosis, Integrin-β1 uptake was significantly enhanced in cells expressing *Numb-Cherry* (Figure 3E, F, I). In contrast, it was substantially inhibited in cells expressing *Opo-GFP* (Figure 3C, D, I). Interestingly, cells co-

expressing both constructs showed a rate of integrin endocytosis that was not significantly different from untransfected cells (Figure 3G-I) or from cells expressing the control *GFP* construct (Figure 3A, B, I). These results show that Opo antagonizes Numb and functions as a negative regulator of integrin endocytosis.

Opo loss-of-function enhances integrin internalization in the medaka optic cup.

To further strengthen our observations from HeLa cells we next set out to investigate the role of Opo in integrin receptors trafficking during optic cup folding. To this end, we carried out *in vivo* FRAP experiments using the medaka eye-specific transgenic line *Vsx3::Integrinβ1Tail-GFP* (Figure S3A). Benefiting from the strictly polarized architecture of the retinal epithelium, we bleached equivalent volumes either at the basal or apical side of both wild type and *opo* mutant retinae (Figure S3). Fluorescence recovery, which occurred at the expense of the unbleached half of the columnar neuroblasts, was monitored in a central optical section of the bleached volume until it achieved a plateau, reflecting that forward and reverse transport of labeled molecules had reached an equilibrium (Figure S3A' and A''). In wild type tissues, FRAP analyses consistently revealed higher and faster integrin recovery at the basal rather than at the apical side (Figure 4A,B; S3A; Movie SM1), thus indicating that integrins are asymmetrically trafficked through the epithelium with a net flux towards the basal side. The analysis of four independent FRAP experiments in mutant tissue showed instead that integrin basal recovery (Figure 4A,B; S3A; Movie SM1) is significantly reduced when compared to the wild type. As a control, the recovery rates for the apical tracer Par3-eGFP (Figure 4C,D; S3B; Movie SM2) are not significantly different from those measured in wild type tissues. These results suggest that *opo* function is specifically required for basal, but not apical, transport of integrins *in vivo*.

Additionally, electron microscopy (EM) studies also support a role for Opo in trafficking during optic cup morphogenesis. Immunogold analysis of stage 23 *Vsx3::eGFP_Opo* retinae revealed that Opo is associated to basal endosomes (Figure S3C,D). Furthermore, morphological EM analysis of stage 23 wild type and *opo* mutant retinae revealed a significant accumulation of intracellular vesicles specifically at the basal end of the mutant neuroblasts (Figure 4E,F; S3E,F). Although collectively our analyses clearly indicate that Opo acts as regulator of integrin trafficking during optic cup folding, they cannot

discriminate whether this is due to an impaired forward transport or an increased endocytic rate.

To address this question, we performed internalization assays *in vivo* using the *Vsx3::Intβ1Tail-GFP* line, as the GFP tag of the fusion protein is oriented towards the extracellular space (Figure 4G-O). To establish the rate of Integrin uptake in both wild-type and *opo* retinae, dechorionated embryos were incubated with α-GFP antibodies for 30 min before fixation. Fluorescence intensity associated to antibody internalization was then quantified in equivalent areas, both at the basal surface and in medial zones of the retina. We found that in *opo Intβ1Tail-GFP* uptake is significantly enhanced in both areas when compared to wild type retinae (Figure 4O), indicating that Opo functions as a negative regulator of integrin endocytosis also during optic cup folding.

Opo and Numb co-localize to the end-feet of the neuroepithelial precursors and regulate basal localization of Integrin-β1

In vertebrates, *numb* and *numbl* have been detected in a wide range of tissues and developmental stages (Wakamatsu et al., 1999; Zhong et al., 1997). In zebrafish embryos both transcripts are ubiquitously expressed before neurulation and get progressively restricted to the anterior nervous system and in particular to the retina (Niikura et al., 2006; Reugels et al., 2006). The analysis of *numb* and *numbl* expression by qPCR and *in situ* hybridization showed comparable profiles in medaka and confirmed that both genes are expressed in the developing retina (Figure S4A-F). Similarly, both *opo* transcripts and Opo protein are enriched at the basal side of the retinal epithelium in vertebrates (Figure S4G-J; Martinez-Morales et al., 2009; Mertes et al., 2009). To investigate *in vivo* the distribution of Opo and Numb during the folding of the optic cup (stage 24), we examined the medaka transgenic lines *Vsx3::eGFP_Opo* and *Vsx3::Numb_eGFP* (Figures 5A,B; S4; Movies SM3, SM4). Confocal microscopy analysis revealed that both proteins are enriched at the basal tip of the neuroblasts in the retina. Numb shows a strong cortical accumulation at the vitreal surface as well as in the baso-lateral cortex of mitotic cells (Figure 5B,C), as previously reported for zebrafish and chick neuroepithelial cells (Reugels et al., 2006; Wakamatsu et al., 1999). Finally, the injection of *Numb_Cherry* RNA into *Vsx3::eGFP_Opo* embryos at one-cell stage confirmed *in vivo* the co-localization of both proteins at the basal surface of

the retinal epithelium (Figure 5D-F). Interestingly, Numb basal localization appeared only mildly reduced in *opo* mutants as visualized in a *Vsx3::Numb_eGFP* background (Figure S4K,L), suggesting that its localization does not depend completely on *opo* function.

It has been shown that Numb regulates Integrin-β turnover *in vitro* (Nishimura and Kaibuchi, 2007; Teckchandani et al., 2009). To determine whether Numb also functions as a regulator of focal adhesions in the retinal epithelium, we generated retinal clones overexpressing *numb* and monitored Integrin-β1 localization (Figure 5G-P). Integrin-β1 recruitment at the basal side of the neuroepithelium was noticeably reduced in *numb* gain-of-function clones (Figure 5K,N) but not in control clones expressing only the *Lyn_tdTomato* tracer (Figure 5H). These results, together with previous findings on *opo* function, suggest that Numb and Opo cooperate to regulate focal adhesions turnover during optic cup formation.

Numb/numbl **gain-of-function impairs optic cup morphogenesis**

A logical prediction to be drawn from the functional antagonism observed between Numb/Numbl and Opo would be that *numb/numbl* gain-of-function should mimic the embryonic phenotype observed in *opo* mutants. To confirm this, and to gain insight into the morphogenetic role of *numb/numbl* during optic cup morphogenesis, we injected medaka *numb* and *numbl* RNAs into medaka embryos at one-cell stage. Injected embryos developed tissue malformations strikingly similar to those observed in *opo* mutants. The injection of 25 ng/µl of either *numb* (Figure. 6A, B) or *numbl* (Figure. 6C, D) RNAs resulted in a proportion of the embryos (19%, n=76 and 12%, n=102, respectively; Figure 6E) in which optic cup folding was impaired. The injection of 100 ng/µl of *numb* or *numbl* RNAs resulted in a higher proportion of affected embryos (34,8 %, n=74 and 36%, n=40, respectively; Figure 6E). Among the morphological defects observed, large ventral openings of the optic cups (Figure 6F, G) as well as strong craniofacial malformations (Figure 6H, I) were particularly prominent in hatchlings. Interestingly, a proportion of embryos injected with the highest dose (100 ng/µl) of *numb* (8,7%; Figure 6E, J) or *numbl* (10%, Figure 6E, K) developed complete cyclopia, a condition also observed in strongly affected *opo* morphants (Martinez-Morales et al., 2009), thus suggesting that Numb and Opo may also cooperate during the bilateralization of the eye field.

To extend our observations to another vertebrate model we also injected *numb* and *numbl* RNAs into zebrafish embryos (evolutionary distance 115-200 Myr (Furutani-Seiki and Wittbrodt, 2004). The injection of either 100 ng/µl of *numb* (n=228) or 50 and 200 ng/µl of *numbl* RNA (n=288 and n=291, respectively) resulted in both a proportion of defects and a phenotypic range of ocular and craniofacial malformations similar to those observed in medaka embryos (Figure S5A-F).

***Numb/numbl* and *opo* interact genetically.**

Given the identified association between Opo and Numb/Numbl proteins, we decided to test whether this interaction was also observed at the genetic level. To this end, *numbl* RNA (25 ng/µl) was injected in the *opo* background. While the percentage of misshapen eyes observed in the progeny of an $opo^{+/-}$ cross is roughly Mendelian (24 ± 0,1 %), and the injection of *numbl* RNA (25 ng/µl) into wild type embryos yields 12% ± 1.1 of retinal defects, when the RNA was injected using the mutant background, ocular malformations increased to 45,8 % ± 0.8 (Figure 6L). This percentage was significantly higher than what is expected from simple additive effects, as determined after analysis by two-way ANOVA of three independent experiments ($P<0.0001$, see raw data in Table S2); thus showing a synergistic effect. Moreover, the injection of *numbl* RNA (25 ng/µl) in the *opo* context resulted in a small proportion (3,3 % ± 1.7) of cyclopic embryos, a phenotype never observed in a wild type background.

To further expand our analysis we tested whether a partial inactivation of *numb/numbl* function may alleviate *opo* ocular phenotype. To this end, we used splicing morpholinos *Mo_numbI4E5* and *Mo_numbII4E5* to specifically knockdown gene expression (Figure S5G, H). In agreement with the severe defects observed in $Numb^{-/-}$ mice (Zhong et al., 2000), the co-injection of both morpholinos at high concentration (300 µM) caused substantial embryo lethality. To overcome this, morpholinos were injected at a lower concentration (50 and 100 µM respectively) into one blastomere at 4-cell stage embryos, both in wild type and *opo* backgrounds. Morpholino co-injection at this concentration did not interfere with optic cup folding. However, it significantly reduced the percentage of embryos (from the expected Mendelian 25% to 15% ± 3) showing the characteristic flattened optic cups observed in *opo* mutants (Figure 6M). In addition, a proportion of the injected

embryos (11,9% ± 0,9) displayed a partial rescue of optic cup morphology, showing an intermediate bending never observed either in *opo* mutants or in wild type siblings (Figures 6N-P'). To support this observation, we measured the folding angles of the retinae and found that rescued embryos showed narrower cup folding angles than mutants (Figure 6N-P').

Finally, to complement our analyses, we examined optic cup morphogenesis *in vivo* in wild type and *numbl*-injected zebrafish embryos. The folding of the retinal epithelium was recorded by time-lapse microscopy in *Vsx3:caaxGFP* embryos, either wild type (Figure 6Q) or injected with *numbl* RNA (25 ng/µl; Figure 6R). Using multi-position image acquisition, tissue morphogenesis was simultaneously monitored in control and injected embryos over approximately 4 hours, starting at 20 hpf. While a similar mitotic rate was observed in control and *numbl*-injected retinae, the constriction of the epithelial sheet was retarded in the treated embryos (Figure 6Q,R; Movie SM5). Collectively, these data indicate that *opo* and *numb/numbl* interact genetically to regulate eye morphogenesis.

Discussion

During organogenesis and tissue remodeling, the regulation of cell adhesive properties determines the morphogenetic behavior of entire epithelial sheets. The basal or baso-lateral localization of integrin receptors in epithelia has long been described as a common theme in vertebrate and invertebrate tissues (Bateman et al., 2001; Schoenenberger et al., 1994). However, the molecular mechanisms controlling the asymmetric turnover of integrin receptors have been poorly explored in the context of epithelial morphogenesis (Schotman et al., 2008).

Taking advantage of the polarized architecture of the vertebrate retina (Figure 7A), we studied the folding of the optic cup as a model system for epithelial basal constriction (Martinez-Morales et al., 2009). Previously, we described that integrins adhesive function is required for optic cup folding and that the morphogenetic protein Opo plays an essential role during this process, albeit through a still uncharacterized molecular mechanism (Martinez-Morales and Wittbrodt, 2009). Here we show that Opo binds to clathrin adaptors Numb and Numbl, and functions as a negative regulator of integrin endocytosis. Our data suggest that Opo plays an important role in the stabilization of focal contacts at the basal surface. Although it is still unclear how tensional forces are generated and applied during optic cup folding, it is likely that focal contacts are required to transmit tensions baso-laterally across the epithelial sheet. A similar requirement has been described during the elongation of the *Drosophila* egg chamber (He et al., 2010).

The PTB domain proteins Numb, Numbl and Dab2 have been described as essential adaptors for clathrin-mediated integrin endocytosis (Caswell et al., 2009; Teckchandani et al., 2009). Consistently, they belong to the set of proteins recruited to focal adhesions in a MyosinII-dependent manner, as detected by proteomic analysis (Kuo et al., 2011). Our yeast two-hybrid assay has identified the interactions of Opo with Numbl (high confidence) and Dab2 (moderate confidence). Further biochemical analyses confirmed the preferential interaction of Opo with the PTB domains of Numb and Numbl, whilst showing a much weaker interaction with Dab2. In migratory cells, it has been proposed that Numb and Dab2 may play non-overlapping roles as integrin endocytosis adaptors; Numb acting at the cell periphery and the leading edge and Dab2 mediating bulk internalization of disengaged

integrins (Nishimura and Kaibuchi, 2007; Teckchandani et al., 2009). Both Numb and Opo have been described as baso-laterally distributed proteins in epithelia (Martinez-Morales et al., 2009; Smith et al., 2007). Furthermore, here we show that Numb and Opo colocalize *in vivo* at the basal surface of the retinal epithelium. In contrast, Dab2 localizes preferentially to the apical surface in epithelia (Collaco et al., 2010). All these observations point to Numb and Numbl, rather than Dab2, as the functional partners of Opo.

The data presented here demonstrate that Opo binding to the PTB domain of Numb/Numbl depends on the conserved NPAF motif. In line with previous findings on the functionality of the integrin NPxF motif (Chen et al., 2006; Czuchra et al., 2006), the conservative mutation of the terminal phenylalanine to tyrosine in Opo does not abolish binding to Numb/Numbl. However, the mutation of this residue (1 out of 1090 aa) to aspartic acid (NPAD) strongly interferes with this interaction. It has been shown in *Drosophila* that Numb also binds the endocytic regulator Sanpodo through an amino-terminal conserved NPAF motif (Tong et al., 2010). The parallels between the vertebrate–specific protein Opo and the insect-specific protein Sanpodo can be further extended as both are fast-evolving proteins (O'Connor-Giles and Skeath, 2003), which include four transmembrane passes near their C-termini. Despite these similarities, there is no significant sequence homology between the two proteins, which suggests an independent evolutionary convergence phenomenon.

Our biochemical analyses, presented in the context of previous findings, are summarized in figure 7B. Considering the molecular structures of Opo and its identified partners, two tentative hypotheses can be envisioned to explain Opo function as a repressor of clathrin-mediated integrin endocytosis. The first possibility encompasses a simple competitive binding mechanism involving Numb/Numbl sequestration by Opo, which in turn results in an inhibition of the integrin internalization process. The second possible mechanism would rely on the high-confidence interaction detected between the Opo C-terminus and the chaperone Hsc70, which has a central role in clathrin disassembly (Sousa and Lafer, 2006). Opo recruitment to integrin clusters at the plasma membrane could therefore mediate the premature disassembly of clathrin structures. These two mechanisms are not mutually exclusive and can operate in parallel to inhibit integrin endocytosis.

The prominent morphogenetic role of polarized receptor trafficking has been acknowledged for both cell-to-cell and cell-to-ECM contacts (Nelson, 2009; Ulrich and Heisenberg, 2009).

Although substantial crosstalk between cadherin-mediated and integrin-mediated adhesions has been described (Papusheva and Heisenberg, 2010), they have been classically implicated in distinct morphogenetic phenomena. Thus, whereas the asymmetric internalization of E-cadherin at adherens junctions has been involved in cell intercalation/rearrangement in epithelia (Levayer et al., 2011; Shaye et al., 2008), integrin trafficking along the front-rear axis has been primarily studied in migratory cells (Caswell et al., 2009; Ezratty et al., 2009). The Opo/Numb-dependent mechanism that we describe here suggests that integrin trafficking along the apico-basal axis also plays an important morphogenetic role in epithelial tissues, particularly in the context of basally driven constrictions.

Experimental procedures

Transgenic lines*:** The medaka lines *Rx2::mYFP, Vsx3:Intβ1tail_eGFP* and *Vsx3::eGFP_Opo* have been previously described (Martinez-Morales et al., 2009). To generate the medaka line *Vsx3::zNumb-eGFP*, the fusion z*Numb(PTBL PRRL):*eGFP (Reugels et al., 2006) was cloned into a *Vsx3* expression vector. The resulting construct was then injected into one-cell stage embryos following standard protocols (Thermes et al., 2002). Tol2 mediated transgenesis (Kawakami, 2007) in combination with multisite gateway technology (Invitrogen) were used to generate the stable zebrafish line *Vsx3::eGFPcaax.* The medaka *Vsx3* promoter was inserted into a *p5E-MCS* entry vector and recombined with the Tol2kit vectors *pME-EGFPCAAX* and *p3E-polyA* into the Tol2 destination vector (Kwan et al., 2007). For a description of the ***expression constructs used see supplemental information.

Opo yeast two-hybrid screening: To elucidate Opo biochemical function we performed a yeast two-hybrid screening. The experimental approach used for baits and library construction, the mating methodology employed for screening and the scoring procedure have been previously described ((Formstecher et al., 2005) Hybrigenics). Briefly, two different baits corresponding to the conserved amino (aa. 1-126) and carboxy terminus (aa 905-1090) of the protein were generated by fusion to LexA in the vector pB29. The resulting fusions, N-OpoN-LexA-C and N-LexA-OpoC-C, were then used to screen a customized medaka cDNA library, cloned into the plasmid pP6 and built from medaka mRNAs (stages 18, 24, 31 and 34). The number of interactions tested was 74.2 millions and 64.8 millions for the amino and carboxy baits respectively. The confidence of these interactions was scored using the Predicted Biological Score program to exclude false positives and promiscuous interactions.

GST pulldowns: Swollen glutathione agarose beads (Sigma, G4510) were incubated with GST fusion proteins in PBS buffer containing 1mM DTT and 0.1% NP-40. The mixture was left rotating at 4ºC for 3-4h with end-to-end mixing. The beads (25 µL) were incubated overnight with 200 µL of pull-down buffer (20 mM Hepes pH 7.9,150 mM NaCl, 0.5 mM EDTA, 10 % Glycerol, 0.1% Triton X-100, 1mM DTT), and 20 µL of the S^{35} radiolabeled protein. Beads were washed 3X with pull-down buffer and the bound proteins were eluted in 50 µL Laemmli buffer. The eluted fractions were resolved on a 10% SDS-PA gel. Dried gels were exposed o/n and the signal was quantified with ImageQuant software (GE Healthcare).

Western blotting (WB) and Co-IP: Extract preparations, co-IP and WB were performed as described (Hurtado et al., 2011). The following antibodies were used: Rabbit polyclonal anti-GFP (ICL); monoclonal anti-c-myc at 1:3000 (9E10, Sigma) and monoclonal anti-GFP at 1:1000 (MAB2003, Abnova).

Site-directed mutagenesis: The mutagenesis was performed following the manufacturers' protocol (Agilent, QuikChange Lightning Multi Site-Directed Mutagenesis Kit, 210515-5) with the following primers: ggcatagataacccagccgacgatggagaaggaagcac (t47g_t48a-NPAD) and gcatagataacccagcctacgatggagaaggaag (t48a-NPAY).

Cell culture and immunofluorescence analysis: HeLa cells and immortalized human pigment epithelial cells RPE-1 (Takara Bio Inc.) were cultured at 37°C in 5% CO2 in DMEM or DMEM/F12 (respectively) supplemented with 10% fetal calf serum. For IF experiments, cells were plated on coverslips the day prior to transfection. Transfections were then performed using Lipofectamine 2000 (Invitrogen) according to the manufacturer´s instructions. After 36 hours at 37°C, cells were fixed in 4% PFA for 20 min and permeabilized (when required) with PBS–0.1% Tween–0.5% Triton X-100 containing 5% FCS for 10 min at RT. After PBS washes, cells were sequentially incubated with appropriate dilutions of the primary antibodies (12 hours at 4°C) and secondary antibodies labeled with Alexa-568 or Alexa-633 (30 minutes at room temperature). After PBS washing, cells were mounted and confocal images acquired on a Leica TCS SPE or a Leica TCS SP5 confocal systems using HCX PL APO 63x1.4 Oil objectives. Image processing was carried out using Leica (LAS), Adobe Photoshop and Image J 10.2 software. The following antibodies were used: Rabbit polyclonal anti-GFP at 1:500 (A-11122, Invitrogen); mouse anti-integrin-β1 at 1:300 (MAB1981, Chemicon); and mouse monoclonal anti-alpha adaptin at 1:300 (ab2807, Abcam).

Internalization assays: The internalization of integrins was studied in HeLa cells as previously described (Nishimura and Kaibuchi, 2007). Briefly, cultures were grown and transfected on PDL-coated coverslips. At 70% confluence live cells were incubated for 30 or 40 min at 37^{o}C with mouse anti-integrin-β1, diluted 1:300 (MAB1981, Chemicon), to allow internalization. Then cells were rinsed in PBS, fixed in PFA and permeabilized. Internalized integrins were detected with anti-mouse Alexa633 or Alexa568 secondary antibodies. Parallel negative controls in which cells were treated either without primary antibodies or without permeabilization yielded no significant signal. To quantify integrin internalization, we measured the mean fluorescence intensity per pixel in neighboring transfected and non-transfected cells of the same field (Image J). After background subtraction, relative endocytosis rate was calculated as the transfected/non-transfected ratio (%). Data represent the mean and SEM of 24 cells measured from two independent experiments.

In vivo internalization of integrins in medaka retinae was studied using the transgenic line *Vsx3::Int1βTailGFP*. In this construct the GFP tag is fused N-terminal to the 70 C-terminal amino acids of Integrinβ1, including the transmembrane and intracellular domains. Medaka wt and opo retinae expressing Intβ1tail:eGFP were dissected in cold PBS 1X. Once the overlying ectoderm was removed to facilitate antibody diffusion, embryos were incubated (30 min at 25ºC) with polyclonal anti-GFP antibodies (ab290, Abcam) diluted 1:300. After fixation and permeabilization, internalized integrins were detected with anti-rabbit Alexa555 secondary antibodies. No significant internalization of the antibody was detected in neighboring tissues lacking Intβ1tail:eGFP expression.

In vivo FRAP analysis: Stage 24 embryos expressing *Intβ1Tail:eGFP* or *Par3:eGFP* embryos were immobilized and scanned in a Leica SP5 confocal microscope. Retinal cells expressing eGFP-tagged proteins were monitored using the 488 line of the SP5 100 mW argon laser at 20% power and bleached at 100% laser power. The bleaching protocol was as follows: 3 pre-bleaching images taken every 3 seconds; 5 bleaching pulses taken every 3

seconds at 100% laser power; 30 post-bleaching images taken every 10 seconds. Equivalent areas in the retina were bleached either at the basal or the apical side of the neuroblasts both for wt and *opo* retinae. Recovery occurring at expenses of the unbleached side was monitored. The average fluorescence intensity per area in each compartment was plotted over time (LAS AF, Leica). To determine the plateau and $t_{1/2}$ values for the different FRAP experiments (n=4) regression analyses were carried out using a one-phase exponential association function in GraphPad Prism5. To analyze the relative recovery at the plateau, the fluorescence value after bleaching was normalized to 1.

Electron Microscopy analyses: For morphological EM analyses, stage 23 and 27 embryos were fixed in 0.05 M sodium cacodylate buffer, pH 7.3, containing 2.5% glutaraldehyde and 2% sucrose for 4 hours at 4 C. Samples were washed in cacodylate buffer and treated consecutively with osmium tetroxide 2% for 40 minutes and uranyl acetate 2% for 30 minutes. After washing in cacodylate buffer, samples were dehydrated in graded (50%, 70%, 80%, 95%, and 100%) ethanol solutions and embedded in Epon. To quantify vesicle number in EM sections, consecutive 25 μm^2 areas in contact with the basal lamina (n=15) or the apical surface (n=6) were analysed in at least 3 embryos.

RNA injections*:* The vectors *pCS2+:Numb* and *pCS2+:Numbl* were used to synthesize medaka *Numb* and *Numbl* capped RNAs. Similarly, the fusions *ASIP/Par-3:eGFP* and *pEGFPC1-(avian) paxillin WT1-559* (Martinez-Morales et al., 2009) were used to generate capped sense RNAs. After linearization of the vectors, capped sense RNAs were synthesized *in vitro* using the mMessage Machine Kit (Ambion). Purified RNA (Qiagen RNeasy) was then injected (25-100 ng/µl) into one-cell stage both in medaka and zebrafish embryos. In clonal analysis experiments, *Numb* RNA (100 ng/µl) together with the lineage tracer Lyn_tdTomato (100 ng/µl), were co-injected into a single blastomere of four to eight-cell stage medaka embryos. Mosaic embryos were then fixed in 4% PFA at stage 24, cryo-protected and sectioned as described (Martinez-Morales et al., 2009). Rabbit polyclonal anti-integrin-β1 antibodies were used at 1:300 (Aviva Systems Biology).

Confocal time lapse analyses: Control and injected 20hpf *Vsx3::caaxGFP* embryos were immobilized in E3 (containing 0.01% tricaine) and embedded in 1% low-melting agarose. Time-lapse analyses were performed on a Nikon A1R microscope with a CFI PlanFluor20xMI N.A.0.75 objective and a 488 nm laser line. Samples were imaged as multiposition time-lapses for 3 hours with a time resolution of 3 min. Several central planes, spanning 40 µm, were selected. Movies were put together with single planes from each Z-stack using ImageJ (NIH).

Statistical analysis**:** Quantitative data are expressed as mean ± SEM. Significant differences among groups were evaluated either by t-tests or Two-Way ANOVA followed by Bonferroni post hoc tests (GraphPad Prism) and indicated when relevant.

Acknowledgments
We thank A. Gonzalez-Reyes, L. Centanin, F. Loosli, JL Gomez-Skarmeta and P. Bovolenta for their critical input, Pam Halley for proof-reading and Rocío Polvillo, Katherina García and Corín Díaz for their excellent technical assistance. The programs “Intramural/CSIC” *200920I212*, Juan de la Cierva and FCT (Portugal) supported OB, MDM and IGR respectively. This work was supported by grants *BFU2008-04362* and *BFU2011-22916*.

Figure Legends

Figure 1. Opo interacts with Numb/Numbl through a conserved N-terminal NPxF motif. (A) A schematic representation of the medaka Opo protein. The black boxes represent four transmembrane passes. (B) Conservation of the N-terminal NPxF sequence from teleosts to mammals. (C) Schematic representation of medaka clathrin adaptors. The PTB containing fragments used for GST-pulldowns are indicated. (D) Coomasie staining (left panel) of recombinantly expressed proteins used for GST-pulldowns. Full length Opo interacts with N-Numb, N-Numbl and N-Dab2 *in vitro*, whereas the Integrin-β1 tail fragment preferentially interacts with Numbl and Dab2 (right panel). (E) Coomasie staining (left panel) of recombinantly expressed N-Opo used for GST-pulldowns of either full length or N-terminal (PTB containing) (S^{35}) Numb, Numbl and Dab2. Both full length and N-terminal Numb and Numbl interact with N-Opo. (F) Western blotting of RPE-1 cellular extracts immunoprecipitated with anti-GFP antibody. Staining with anti-GFP and anti-Myc antibodies confirms the interaction of GFP-Opo and Myc-Numbl in RPE-1 cells. GFP alone was used as a negative control in parallel experiments (G) Colocalization of Numb_Cherry and OpoA_GFP at the cellular cortex in HeLa cells. (H) GST pulldowns of S^{35}-labelled F46Y and F46D Opo mutants shows reduced interaction with N-Numb and N-Numbl. (I) Quantification of wild type Opo, F46Y-Opo and F46D-Opo binding to N-Numb/N-Numbl in GST pulldowns. Input lines contain 10% of the input. Error bars represent SEM of three experiments. Bar= 20 µm. See also Figure S1 and Table S1.

Figure 2. Opo localizes to Ap2α-positive clathrin-coated structures (CCS). (A-C) HeLa cells transfected either with mouse GFP-OpoA or C-terminal and N-terminal Opo truncations (A) were stained with anti- Ap2α antibodies to detect CCS. Cells transfected with GFP-OpoA (B-D) show colocalization (arrows) at the cellular cortex (arrows in xz and xy projections). This is reduced when GFP-OpoA_ΔC (E-G) or GFP-OpoB (H-J) are transfected Bars= 5 µm

Figure 3. Opo inhibits Integrin β1 internalization in HeLa cells. (A) HeLa cells expressing control GFP (*pCS2+:GFP*) stained with: (B) anti-integrin-β1 antibodies after the internalization assay. (C) Opo-GFP expressing cells stained with: (D) anti-integrin-β1 antibodies after the internalization assay display a significant reduction in Integrin-β1 uptake. (E-F) In contrast Integrin-β1 uptake is enhanced in cells expressing Numb-Cherry constructs. Cells co-expressing both constructs are shown in (G-H). Dotted lines represent areas of measured Integrin-β1 turnover. White and pink asterisks denote equivalent transfected and non-transfected cells respectively. (I) Relative endocytosis rate is expressed as the transfected/non-transfected ratio (%). Data represent the mean and SEM of 24 cells in each condition. Bar= 25 µm

Figure 4. Integrinβ1 endocytosis is enhanced in the *opo* retina. *In vivo* FRAP reveals altered integrin-β1 trafficking in *opo* mutants**.** Equivalent areas were bleached from either basal or apical sides, in stage 24 wild type and *opo* retinae (see Figure S3 for experimental details). (A-D) Statistical analysis of FRAP experiments. The plateau (A, C) and $t_{1/2}$ (B, D) values for the different FRAP experiments are shown. Quantitative data are expressed as mean ± SEM. Significant differences among groups were evaluated by t-tests and indicated

when relevant. Notice that when wild type and *opo* data are compared, significant differences were observed only for the basal recovery of *Intβ1Tail-eGFP* (A,B) but not for *Par3-eGFP* (C,D). (E-F) EM analysis of stage 23 wild type and *opo* retinas reveals an accumulation of intracellular vesicles at the basal feet of the mutant neuroblasts (see Figure S3 for experimental details). Quantitative data at the basal (E) and apical (F) regions are provided for a 25 square µm area (n=15). Vesicles were classified according to their size. As an internal control mitochondria numbers were also recorded. Significant differences among groups were evaluated by t-tests (GraphPad Prism) and indicated when relevant. Error bars represent SEM. (G-O) In vivo internalization of integrins in the retina. Optical sections from wt (G-I,M-N) and *opo* (J-L) *Vsx3::Int1βTailGFP* retinae stained with: DAPI (G,I,J,L,M) and anti-GFP antibody (H-I,K-L,N) after Integrin-β1 uptake assays. Anti-Integrinβ1Tail-GFP staining is significantly increased in *opo* mutants (K-L,O), indicating an increased endocytic rate. No significant internalization of the antibody was detected in tissues not expressing the construct (compare red and white arrows in N). Dotted lines (H,K) represent areas of measured Integrin-β1 turnover (basal membrane and mid-retina). (O) Relative endocytosis rate is expressed as Average Pixel Intensity (API). Data represents the mean and SEM of 6 embryos in each condition. Bar=10µm

Figure 5. Numb colocalizes with Opo and regulates integrin recruitment at the basal retina. (A-B) Confocal microscopy analysis of transgenic medaka lines *Vsx3::eGFP_Opo* and *Vsx3::Numb_eGFP* shows the localization of both proteins at the basal end of the neuroblast. See also SM5 and SM6 (C) Numb_eGFP displays strong accumulation both at the basal surface (white arrow) and the baso-lateral cortex of mitotic cells (red arrow). (D-F) Transient expression of *Numb_Cherry* RNA in *Vsx3::eGFP_Opo* embryos shows the *in vivo* co-localization of Numb and Opo at the basal surface. (G-P) Stage 24 retinal sections showing different clones overexpressing either the linage tracer *Lyn_tdTomato* (G-I) or *numb* together with *Lyn_tdTomato* (J, L). Higher magnification pictures of J-L are shown in M-O. Note that Integrin-β1 basal enrichment is reduced (yellow arrows) in *numb* gain-of-function clones as assessed by immunostaining (K, N). Integrin-β1 and Lyn_tdTomato are quantified (n=5) in 10µm^2 basal areas and are expressed as mean ± SEM (P). nr= neural retina; b=basal; L=lens.

Figure 6. Numb/Numbl and Opo interact genetically in medaka embryos. (A-B) Injection of 25 ng/µl of *numb* RNA in medaka embryos results in a flat eye phenotype (red arrows), similar to that observed in *opo* mutants (inset). (C-D) Overexpression of *numbl* RNA (25 ng/µl) generates similar tissue malformations. (E) Percentage of phenotypic malformations upon injection of increasing amounts of *numb* or *numbl* RNAs in medaka. Note that some of the embryos injected with 100 ng/µl displayed cyclopia. (F-I) Medaka embryos injected with *numbl* (100 ng/µl) show large ventral openings of the optic cup and severe cranio-facial malformations (arrows). (J-K) A small proportion of embryos injected with 100 ng/µl of *numb* or *numbl* developed complete cyclopia. (L) Statistical analysis showing a synergistic effect when n*umbl* RNA (25 ng/µl) was injected into an *opo* mutant background. Note the increased % of malformations over the expected 25% from the heterozygous cross. (M) Statistical analysis showing that co-injection of splicing morpholinos targeting *numb* and *numbl* partially rescues ocular malformations observed in *opo* mutants. (E, L-M) Error bars represent SEM. (N-P') Ocular morphology in wild type (N, N'), partially rescued (O, O') and

opo (P, P') medaka embryos from stage 23. Lateral views (N-P). Dorsal views (N'-P'). Ocular morphology is highlighted with dotted lines both for the left (yellow line) and right (white lines) eyes. Optic cup (oc) folding angle is indicated in N-P. f= forebrain. Folding of the retinal epithelium examined by time-lapse confocal microscopy in Vsx3:caaxGFP transgenic embryos. The basal constriction of the epithelial sheet is significantly impaired in embryos injected with 25 ng/µl of *numbl* RNA (Q) when compared to controls (R). Optic cup folding angle is also indicated. See also Table S2 and movie SM7.

Figure 7. Numb/Numbl and Opo localization and function in the retinal epithelium. (A) Representation of the polarized retinal organization during morphogenesis. Apical and basal polarity cues are represented. Basal localization of integrins, Opo and Numbl at the basal feet of neruroblast cells is also depicted. (A') Paxilin-eGFP is shown to illustrate the enrichment of focal adhesions (FAA) at the basal retina. (B) Schematic diagram of the molecular interactions between Opo, clathrin adaptors and integrins. The PTB domains of talin and clathrin adaptors (Numb, Numbl and Dab2), as well as the NPxF and NPxY motives of Opo and Integrins are depicted.

References

Bateman, J., Reddy, R.S., Saito, H., and Van Vactor, D. (2001). The receptor tyrosine phosphatase Dlar and integrins organize actin filaments in the Drosophila follicular epithelium. Curr Biol *11*, 1317-1327.

Bryant, D.M., and Mostov, K.E. (2008). From cells to organs: building polarized tissue. Nat Rev Mol Cell Biol *9*, 887-901.

Calderwood, D.A., Fujioka, Y., de Pereda, J.M., Garcia-Alvarez, B., Nakamoto, T., Margolis, B., McGlade, C.J., Liddington, R.C., and Ginsberg, M.H. (2003). Integrin beta cytoplasmic domain interactions with phosphotyrosine-binding domains: a structural prototype for diversity in integrin signaling. Proc Natl Acad Sci U S A *100*, 2272-2277.

Caswell, P.T., Vadrevu, S., and Norman, J.C. (2009). Integrins: masters and slaves of endocytic transport. Nat Rev Mol Cell Biol *10*, 843-853.

Chang, H.C., Newmyer, S.L., Hull, M.J., Ebersold, M., Schmid, S.L., and Mellman, I. (2002). Hsc70 is required for endocytosis and clathrin function in Drosophila. J Cell Biol *159*, 477-487.

Chen, H., Zou, Z., Sarratt, K.L., Zhou, D., Zhang, M., Sebzda, E., Hammer, D.A., and Kahn, M.L. (2006). In vivo beta1 integrin function requires phosphorylation-independent regulation by cytoplasmic tyrosines. Genes Dev *20*, 927-932.

Collaco, A., Jakab, R., Hegan, P., Mooseker, M., and Ameen, N. (2010). Alpha-AP-2 directs myosin VI-dependent endocytosis of cystic fibrosis transmembrane conductance regulator chloride channels in the intestine. J Biol Chem *285*, 17177-17187.

Czuchra, A., Meyer, H., Legate, K.R., Brakebusch, C., and Fassler, R. (2006). Genetic analysis of beta1 integrin "activation motifs" in mice. J Cell Biol *174*, 889-899.

Dho, S.E., Trejo, J., Siderovski, D.P., and McGlade, C.J. (2006). Dynamic regulation of mammalian numb by G protein-coupled receptors and protein kinase C activation: Structural determinants of numb association with the cortical membrane. Mol Biol Cell *17*, 4142-4155.

Dong, B., Deng, W., and Jiang, D. (2011). Distinct cytoskeleton populations and extensive crosstalk control Ciona notochord tubulogenesis. Development *138*, 1631-1641.

Ezratty, E.J., Bertaux, C., Marcantonio, E.E., and Gundersen, G.G. (2009). Clathrin mediates integrin endocytosis for focal adhesion disassembly in migrating cells. J Cell Biol *187*, 733-747.

Filardo, E.J., Brooks, P.C., Deming, S.L., Damsky, C., and Cheresh, D.A. (1995). Requirement of the NPXY motif in the integrin beta 3 subunit cytoplasmic tail for melanoma cell migration in vitro and in vivo. J Cell Biol *130*, 441-450.

Formstecher, E., Aresta, S., Collura, V., Hamburger, A., Meil, A., Trehin, A., Reverdy, C., Betin, V., Maire, S., Brun, C.*, et al.* (2005). Protein interaction mapping: a Drosophila case study. Genome Res *15*, 376-384.

Furutani-Seiki, M., and Wittbrodt, J. (2004). Medaka and zebrafish, an evolutionary twin study. Mech Dev *121*, 629-637.

Gutzman, J.H., Graeden, E.G., Lowery, L.A., Holley, H.S., and Sive, H. (2008). Formation of the zebrafish midbrain-hindbrain boundary constriction requires laminin-dependent basal constriction. Mech Dev *125*, 974-983.

He, L., Wang, X., Tang, H.L., and Montell, D.J. (2010). Tissue elongation requires oscillating contractions of a basal actomyosin network. Nat Cell Biol *12*, 1133-1142.

Huang, E.J., Li, H., Tang, A.A., Wiggins, A.K., Neve, R.L., Zhong, W., Jan, L.Y., and Jan, Y.N. (2005). Targeted deletion of numb and numblike in sensory neurons reveals their essential functions in axon arborization. Genes Dev *19*, 138-151.
Hurtado, L., Caballero, C., Gavilan, M.P., Cardenas, J., Bornens, M., and Rios, R.M. (2011). Disconnecting the Golgi ribbon from the centrosome prevents directional cell migration and ciliogenesis. J Cell Biol *193*, 917-933.
Kawakami, K. (2007). Tol2: a versatile gene transfer vector in vertebrates. Genome Biol *8 Suppl 1*, S7.
Knoblich, J.A., Jan, L.Y., and Jan, Y.N. (1995). Asymmetric segregation of Numb and Prospero during cell division. Nature *377*, 624-627.
Kolsch, V., Seher, T., Fernandez-Ballester, G.J., Serrano, L., and Leptin, M. (2007). Control of Drosophila gastrulation by apical localization of adherens junctions and RhoGEF2. Science *315*, 384-386.
Kuo, J.C., Han, X., Hsiao, C.T., Yates, J.R., 3rd, and Waterman, C.M. (2011). Analysis of the myosin-II-responsive focal adhesion proteome reveals a role for beta-Pix in negative regulation of focal adhesion maturation. Nat Cell Biol *13*, 383-393.
Kwan, K.M., Fujimoto, E., Grabher, C., Mangum, B.D., Hardy, M.E., Campbell, D.S., Parant, J.M., Yost, H.J., Kanki, J.P., and Chien, C.B. (2007). The Tol2kit: a multisite gateway-based construction kit for Tol2 transposon transgenesis constructs. Dev Dyn *236*, 3088-3099.
Lecuit, T., and Lenne, P.F. (2007). Cell surface mechanics and the control of cell shape, tissue patterns and morphogenesis. Nat Rev Mol Cell Biol *8*, 633-644.
Letizia, A., Sotillos, S., Campuzano, S., and Llimargas, M. (2011). Regulated Crb accumulation controls apical constriction and invagination in Drosophila tracheal cells. J Cell Sci *124*, 240-251.
Levayer, R., Pelissier-Monier, A., and Lecuit, T. (2011). Spatial regulation of Dia and Myosin-II by RhoGEF2 controls initiation of E-cadherin endocytosis during epithelial morphogenesis. Nat Cell Biol *13*, 529-540.
Martin, A.C., Kaschube, M., and Wieschaus, E.F. (2009). Pulsed contractions of an actin-myosin network drive apical constriction. Nature *457*, 495-499.
Martinez-Morales, J.R., Rembold, M., Greger, K., Simpson, J.C., Brown, K.E., Quiring, R., Pepperkok, R., Martin-Bermudo, M.D., Himmelbauer, H., and Wittbrodt, J. (2009). ojoplano-mediated basal constriction is essential for optic cup morphogenesis. Development *136*, 2165-2175.
Martinez-Morales, J.R., and Wittbrodt, J. (2009). Shaping the vertebrate eye. Curr Opin Genet Dev *19*, 511-517.
Mertes, F., Martinez-Morales, J.R., Nolden, T., Sporle, R., Wittbrodt, J., Lehrach, H., and Himmelbauer, H. (2009). Cloning of mouse ojoplano, a reticular cytoplasmic protein expressed during embryonic development. Gene Expr Patterns *9*, 562-567.
Montell, D.J. (2008). Morphogenetic cell movements: diversity from modular mechanical properties. Science *322*, 1502-1505.
Nelson, W.J. (2009). Remodeling epithelial cell organization: transitions between front-rear and apical-Basal polarity. Cold Spring Harbor Perspect Biol *1*, a000513.
Niikura, Y., Tabata, Y., Tajima, A., Inoue, I., Arai, K., and Watanabe, S. (2006). Zebrafish Numb homologue: phylogenetic evolution and involvement in regulation of left-right asymmetry. Mech Dev *123*, 407-414.

Nishimura, T., and Kaibuchi, K. (2007). Numb controls integrin endocytosis for directional cell migration with aPKC and PAR-3. Dev Cell *13*, 15-28.
O'Connor-Giles, K.M., and Skeath, J.B. (2003). Numb inhibits membrane localization of Sanpodo, a four-pass transmembrane protein, to promote asymmetric divisions in Drosophila. Dev Cell *5*, 231-243.
Papusheva, E., and Heisenberg, C.P. (2010). Spatial organization of adhesion: force-dependent regulation and function in tissue morphogenesis. EMBO J *29*, 2753-2768.
Rasin, M.R., Gazula, V.R., Breunig, J.J., Kwan, K.Y., Johnson, M.B., Liu-Chen, S., Li, H.S., Jan, L.Y., Jan, Y.N., Rakic, P.*, et al.* (2007). Numb and Numbl are required for maintenance of cadherin-based adhesion and polarity of neural progenitors. Nat Neurosci *10*, 819-827.
Reugels, A.M., Boggetti, B., Scheer, N., and Campos-Ortega, J.A. (2006). Asymmetric localization of Numb:EGFP in dividing neuroepithelial cells during neurulation in Danio rerio. Dev Dyn *235*, 934-948.
Santolini, E., Puri, C., Salcini, A.E., Gagliani, M.C., Pelicci, P.G., Tacchetti, C., and Di Fiore, P.P. (2000). Numb is an endocytic protein. J Cell Biol *151*, 1345-1352.
Sawyer, J.M., Harrell, J.R., Shemer, G., Sullivan-Brown, J., Roh-Johnson, M., and Goldstein, B. (2010). Apical constriction: a cell shape change that can drive morphogenesis. Dev Biol *341*, 5-19.
Schoenenberger, C.A., Zuk, A., Zinkl, G.M., Kendall, D., and Matlin, K.S. (1994). Integrin expression and localization in normal MDCK cells and transformed MDCK cells lacking apical polarity. J Cell Sci *107 (Pt 2)*, 527-541.
Schotman, H., Karhinen, L., and Rabouille, C. (2008). dGRASP-mediated noncanonical integrin secretion is required for Drosophila epithelial remodeling. Dev Cell *14*, 171-182.
Shaye, D.D., Casanova, J., and Llimargas, M. (2008). Modulation of intracellular trafficking regulates cell intercalation in the Drosophila trachea. Nat Cell Biol *10*, 964-970.
Smith, C.A., Lau, K.M., Rahmani, Z., Dho, S.E., Brothers, G., She, Y.M., Berry, D.M., Bonneil, E., Thibault, P., Schweisguth, F.*, et al.* (2007). aPKC-mediated phosphorylation regulates asymmetric membrane localization of the cell fate determinant Numb. Embo J *26*, 468-480.
Solon, J., Kaya, A., Colombelli, J., and Brunner, D. (2009). Pulsed forces timed by a ratchet-like mechanism drive directed tissue movement during dorsal closure. Cell *137*, 1331-1342.
Sousa, R., and Lafer, E.M. (2006). Keep the traffic moving: mechanism of the Hsp70 motor. Traffic *7*, 1596-1603.
Teckchandani, A., Toida, N., Goodchild, J., Henderson, C., Watts, J., Wollscheid, B., and Cooper, J.A. (2009). Quantitative proteomics identifies a Dab2/integrin module regulating cell migration. J Cell Biol *186*, 99-111.
Thermes, V., Grabher, C., Ristoratore, F., Bourrat, F., Choulika, A., Wittbrodt, J., and Joly, J.S. (2002). I-SceI meganuclease mediates highly efficient transgenesis in fish. Mech Dev *118*, 91-98.
Tong, X., Zitserman, D., Serebriiskii, I., Andrake, M., Dunbrack, R., and Roegiers, F. (2010). Numb independently antagonizes Sanpodo membrane targeting and Notch signaling in Drosophila sensory organ precursor cells. Mol Biol Cell *21*, 802-810.
Ulrich, F., and Heisenberg, C.P. (2009). Trafficking and cell migration. Traffic *10*, 811-818.
Ungewickell, E.J., and Hinrichsen, L. (2007). Endocytosis: clathrin-mediated membrane budding. Curr Opin Cell Biol *19*, 417-425.

Wakamatsu, Y., Maynard, T.M., Jones, S.U., and Weston, J.A. (1999). NUMB localizes in the basal cortex of mitotic avian neuroepithelial cells and modulates neuronal differentiation by binding to NOTCH-1. Neuron *23*, 71-81.
Wang, Z., Sandiford, S., Wu, C., and Li, S.S. (2009). Numb regulates cell-cell adhesion and polarity in response to tyrosine kinase signalling. EMBO J *28*, 2360-2373.
Wu, M., Smith, C.L., Hall, J.A., Lee, I., Luby-Phelps, K., and Tallquist, M.D. (2010). Epicardial spindle orientation controls cell entry into the myocardium. Dev Cell *19*, 114-125.
Zhong, W., Jiang, M.M., Schonemann, M.D., Meneses, J.J., Pedersen, R.A., Jan, L.Y., and Jan, Y.N. (2000). Mouse numb is an essential gene involved in cortical neurogenesis. Proc Natl Acad Sci U S A *97*, 6844-6849.
Zhong, W., Jiang, M.M., Weinmaster, G., Jan, L.Y., and Jan, Y.N. (1997). Differential expression of mammalian Numb, Numblike and Notch1 suggests distinct roles during mouse cortical neurogenesis. Development *124*, 1887-1897.
Zhou, P., Alfaro, J., Chang, E.H., Zhao, X., Porcionatto, M., and Segal, R.A. (2011). Numb links extracellular cues to intracellular polarity machinery to promote chemotaxis. Dev Cell *20*, 610-622.

Figure 1

Click here to download high resolution image

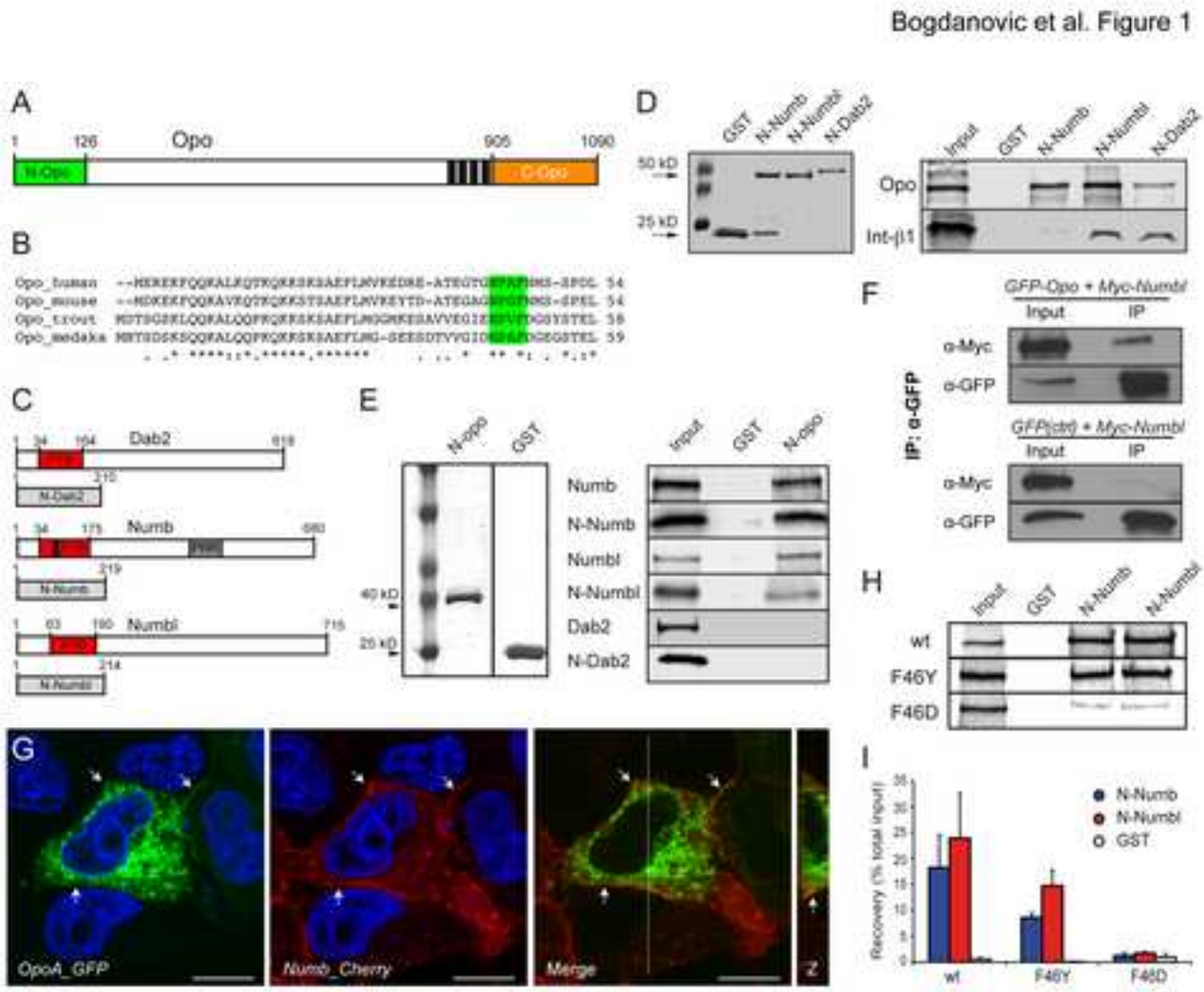

Figure 2

Click here to download high resolution image

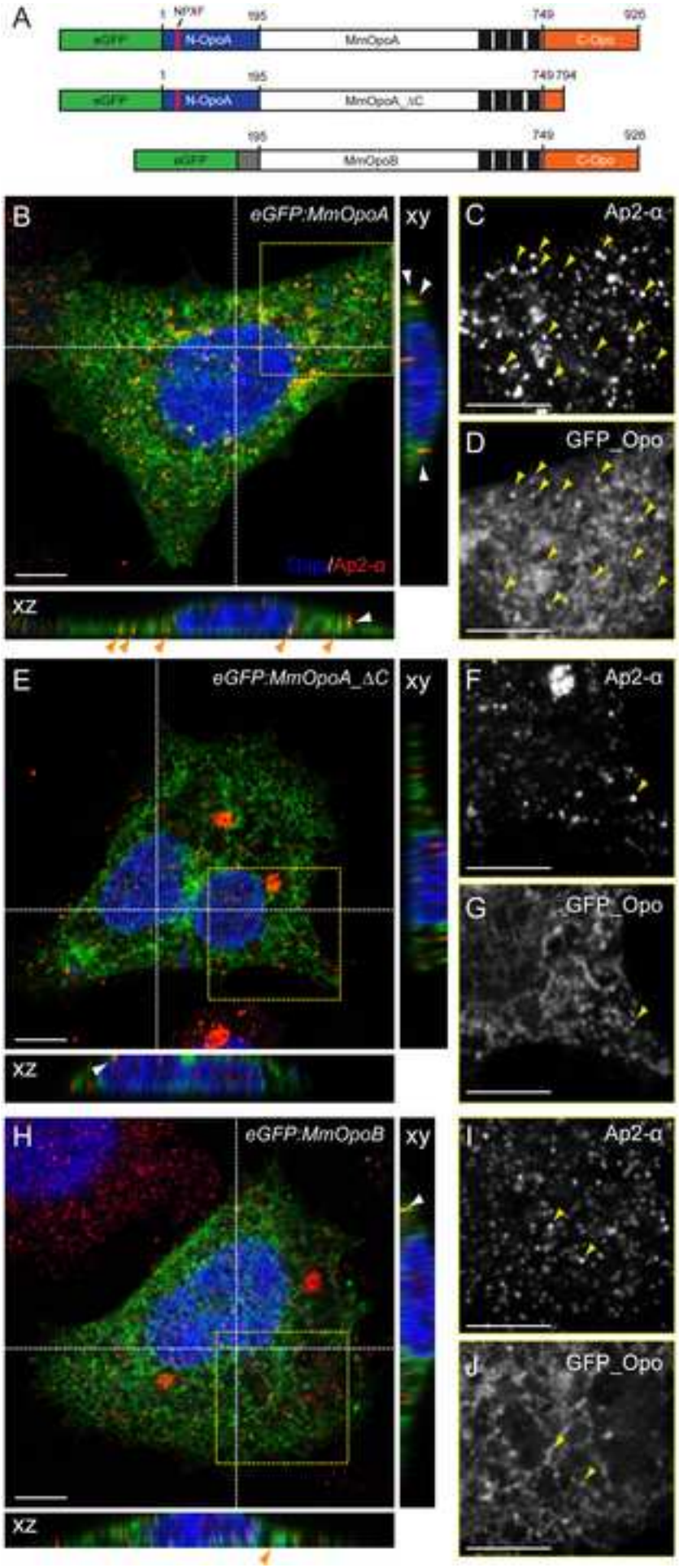

Bogdanovic et al. Figure 2

Figure 3

Click here to download high resolution image

Bogdanovic et al. Figure 3

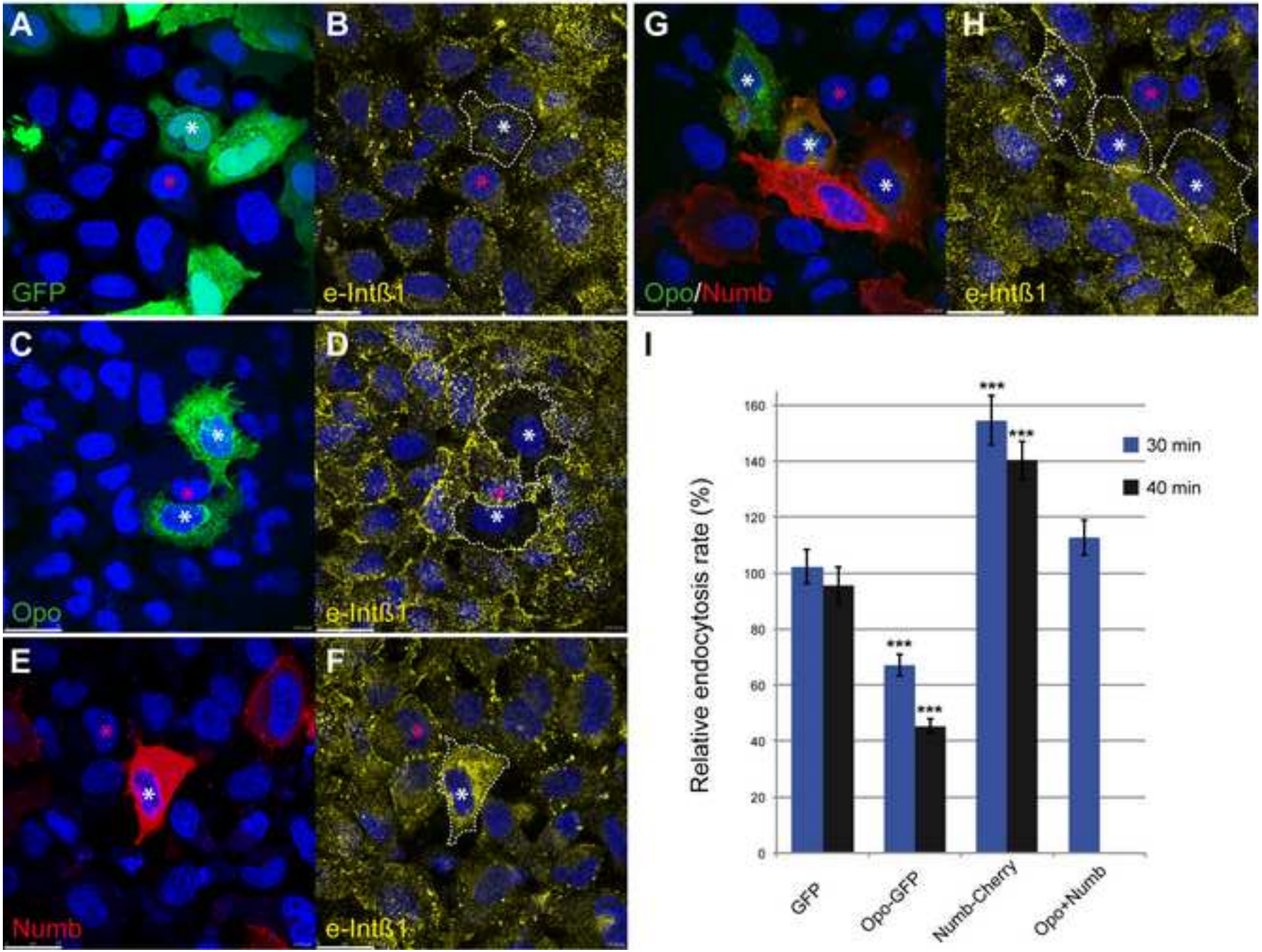

Figure 4

Click here to download high resolution image

Bogdanovic et al. Figure 4

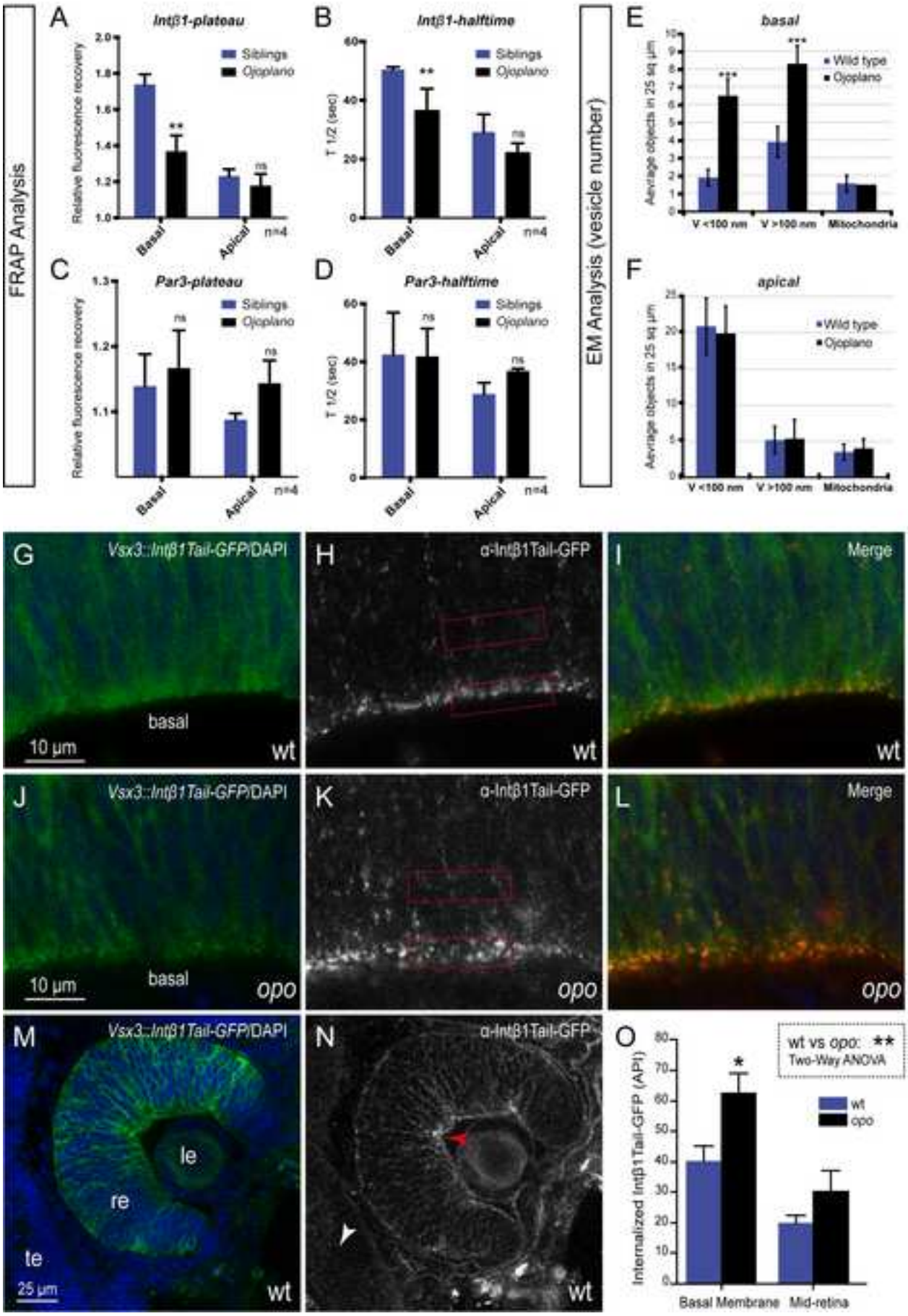

Figure 5

Click here to download high resolution image

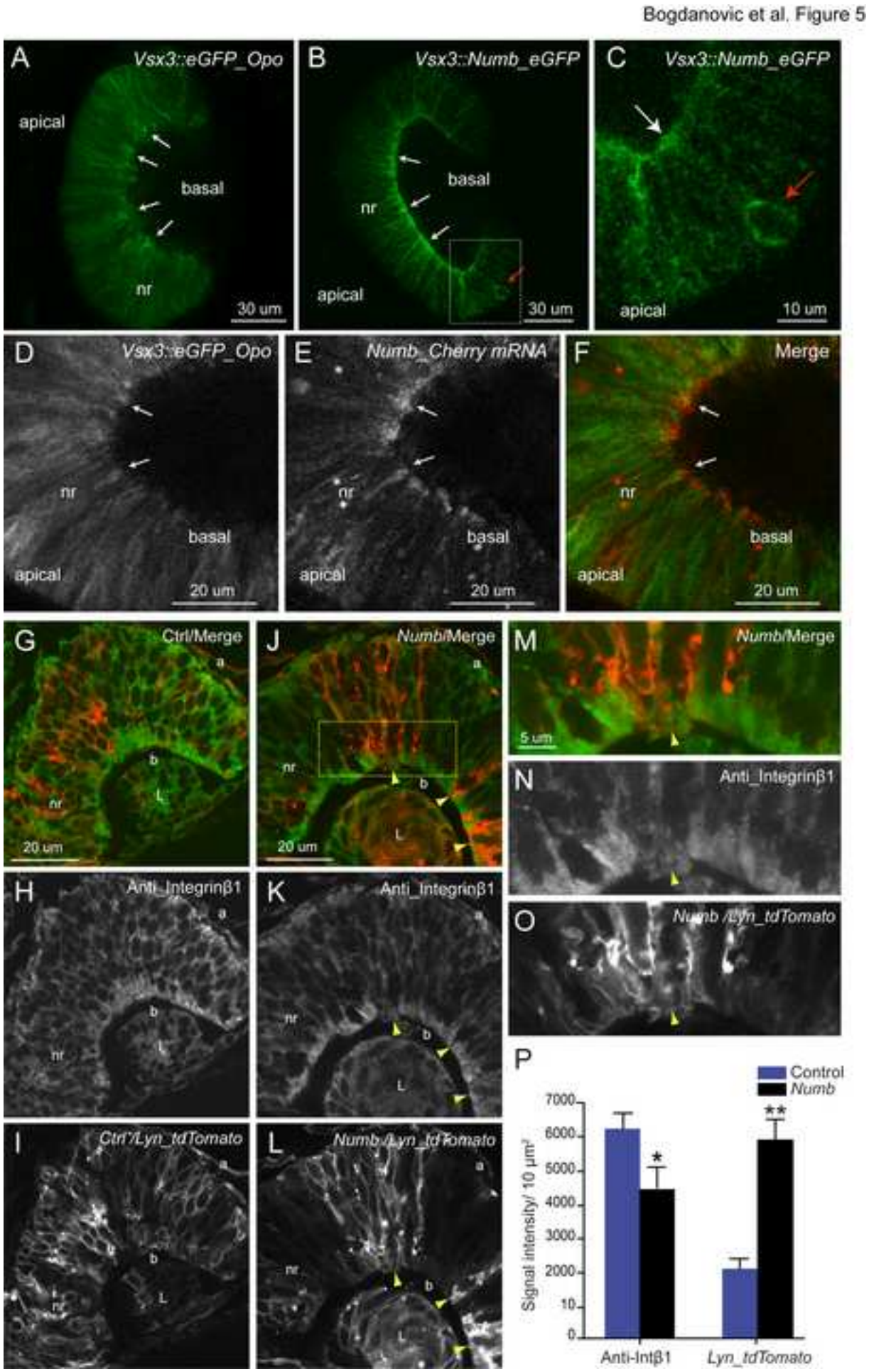

Figure 6

Click here to download high resolution image

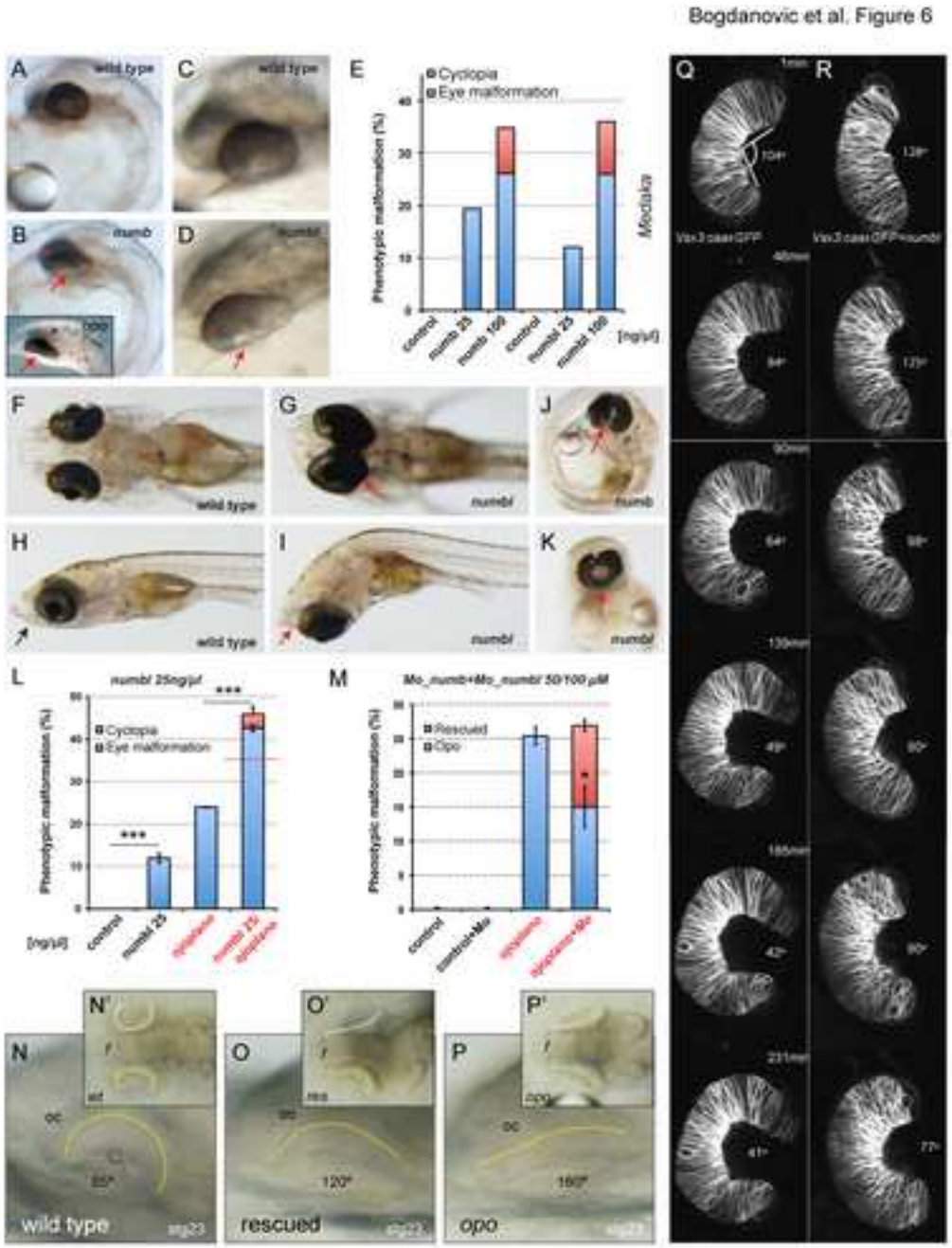

Figure 7
Click here to download high resolution image

Bogdanovic et al. Figure 7

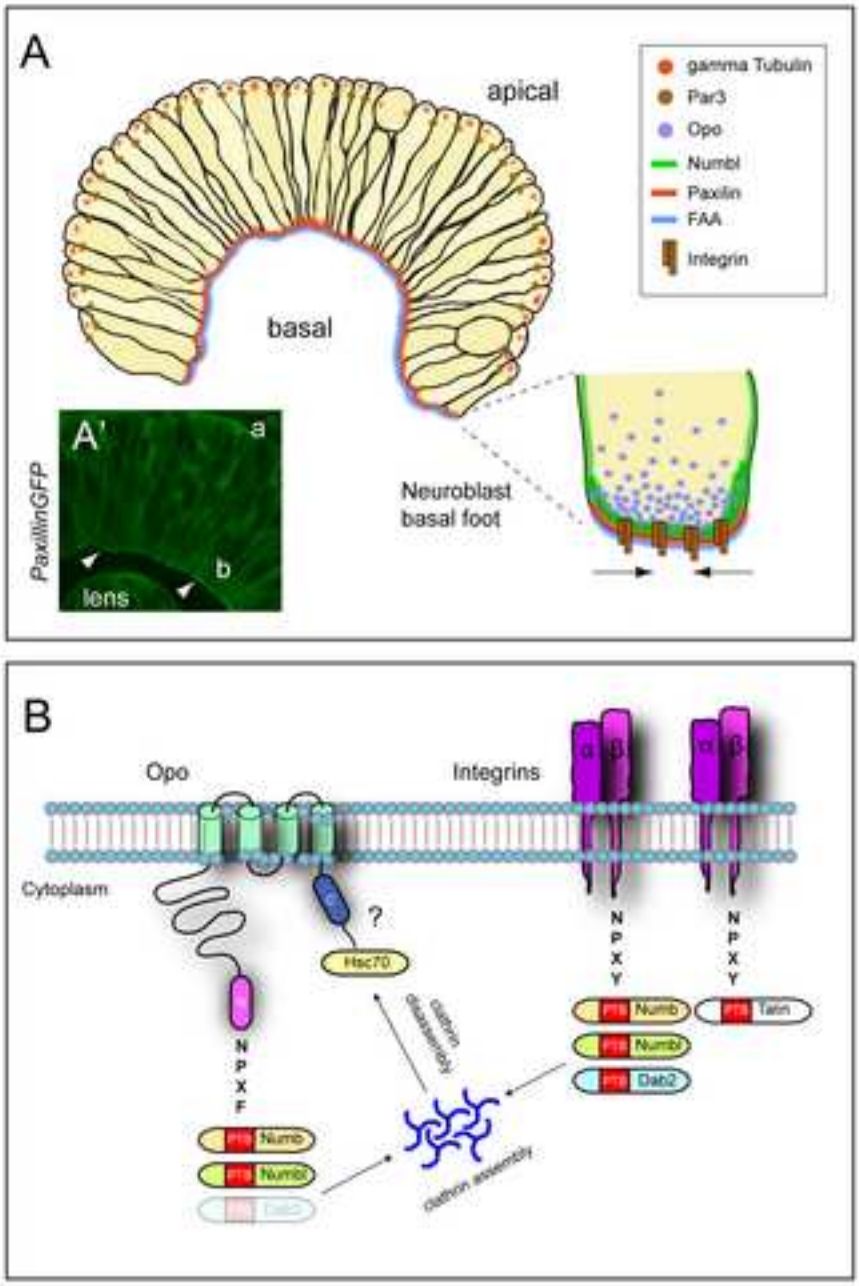

Inventory of Supplemental information.

Bogdanovic et al: *Numb/Numbl-Opo antagonism controls retinal epithelium morphogenesis by regulating integrin endocytosis*

Supplemental Data Includes 2 Tables, 5 figures and 5 Supplemental movies.

List of Supplemental Items and correspondence to main figures.

In relation to Figure 1:

Figure S1. Confirmation of Opo protein topology by epitope tagging

Table S1. List of Y2H highest-scoring proteins for Opo baits

In relation to Figure 2:

Figure S2. *Opo-GFP localizes to Ap2α-positive clathrin-coated structures (CCS)*

In relation to Figure 4:

Figure S3: FRAP experiments and EM analyses showing Opo function as a regulator of integrin trafficking

Movies SM1 and SM2: FRAP analysis of *Intß1tail-eGFP* and *Par3-eGFP* in wild type and *opo* mutant retinae

In relation to Figure 5:

Figure S4. *Numb, numbl and opo* expression in teleost embryos.

Movies SM3 and SM4. In vivo localization of *eGFP-Opo* and *Numb-eGFP* in the medaka retina during morphogenesis.

In relation to Figure 6:

Table S2. Raw data showing *opo* and numb/*numbl* genetic interaction

Movie SM5. Confocal time-lapse analysis of optic cup folding in *wt* and *numbl*-overexpressing embryos

Figure S5. Opo and numb/*numbl* genetic interaction.

Supplemental Online Material

Numb/Numbl-Opo antagonism controls retinal epithelium morphogenesis by regulating integrin endocytosis

Bogdanoviç O[1]*, Delfino-Machín M[1]*, Nicolás-Pérez M[1], Gavilán MP[2], Gago-Rodrigues I[1], Fernández-Miñán A[1], Lillo C[3], Rios RM[2], Wittbrodt J[4], Martínez-Morales JR[1#]*.

1. Centro Andaluz de Biología del Desarrollo (CSIC/UPO/JA), 41013 Sevilla, Spain
2. CABIMER (CSIC), 41092 Sevilla, Spain
3. INCYL (University of Salamanca), 37007 Salamanca, Spain
4. COS, Heidelberg University and ITG, Karslruhe Institute of Technology, Germany
*Equal contribution
[#]Correspondence: jrmarmor@upo.es

(Supplemental Data includes: 5 Figures, 2 Tables and 5 Supplemental Movies).

Inventory of Supplemental information.

In relation to Figure 1:
-*Figure S1.* Confirmation of Opo protein topology by epitope tagging
-*Table S1.* List of Y2H highest-scoring proteins for Opo baits

In relation to Figure 2:
-*Figure S2*. *Opo-GFP localizes to Ap2α-positive clathrin-coated structures (CCS)*

In relation to Figure 4:
-*Figure S3:* FRAP experiments and EM analyses showing Opo function as a regulator of integrin trafficking
-*Movies SM1 and SM2:* FRAP analysis of *Intß1tail-eGFP* and *Par3-eGFP* in wild type and *opo* mutant retinae

In relation to Figure 5:
-*Figure S4*. *Numb, numbl and opo* expression in teleost embryos.
-*Movies SM3 and SM4.* In vivo localization of *eGFP-Opo* and *Numb-eGFP* in the medaka retina during morphogenesis.

In relation to Figure 6:
-*Table S2*. Raw data showing *opo* and numb/*numbl* genetic interaction
-*Movie SM5*. Confocal time-lapse analysis of optic cup folding in *wt* and *numbl*-overexpressing embryos
-*Figure S5. Opo* and numb/*numbl* genetic interaction.

Bogdanovic et al. Supplementary Fig 1

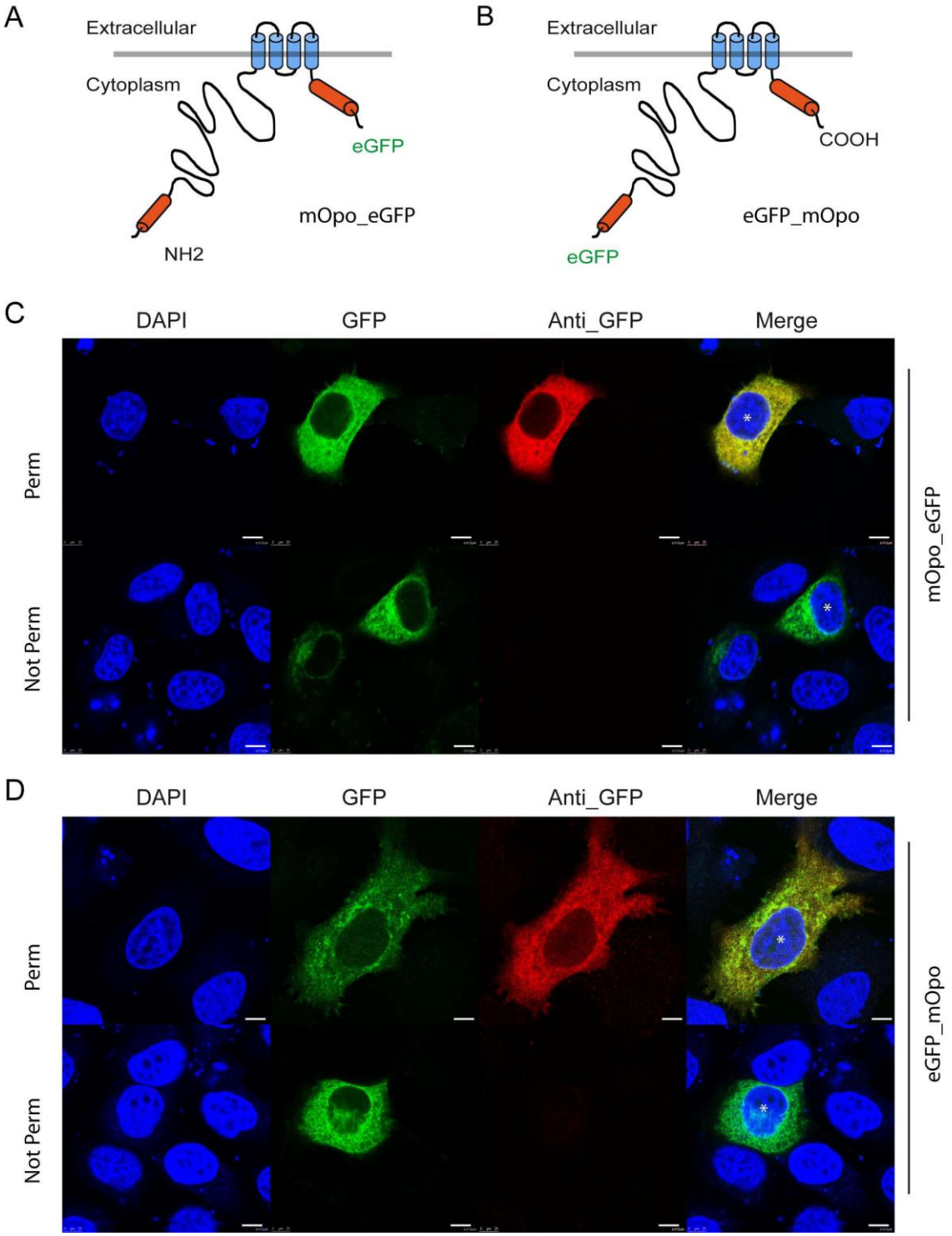

Figure S1. *Confirmation of Opo protein topology by epitope tagging.*
Conservation of Opo C and N-termini was analyzed using blastp and tblastn. Taking the medaka Opo N-terminal sequence as a reference query, analyses only detected significant sequence homology within the vertebrate group. In contrast, similar analyses using the medaka Opo C-terminal sequence identified homology in several metazoan groups including cnidarians and echinoderms. Interestingly, no homology has found with the protostome group. Conserved amino and carboxyl terminal domains are indicated in orange (A, B). Topology algorithms (Sosui and Phobious) predict four putative transmembrane domains in Opo, with both conserved termini of the protein being oriented towards the cytoplasm. To confirm the predicted topology, we carried out immunofluorescence assays in HeLa cells expressing Opo fusions tagged with eGFP either at the C- (A, C) or the N-terminus of the protein (B, D). Transfected cells were then permeabilized or left untreated before fixation in 4% PFA, immunostained with anti-GFP antibodies and counterstained with DAPI. These analyses corroborate the cytoplasmic orientation of Opo C and N-termini. Bar= 25 µm

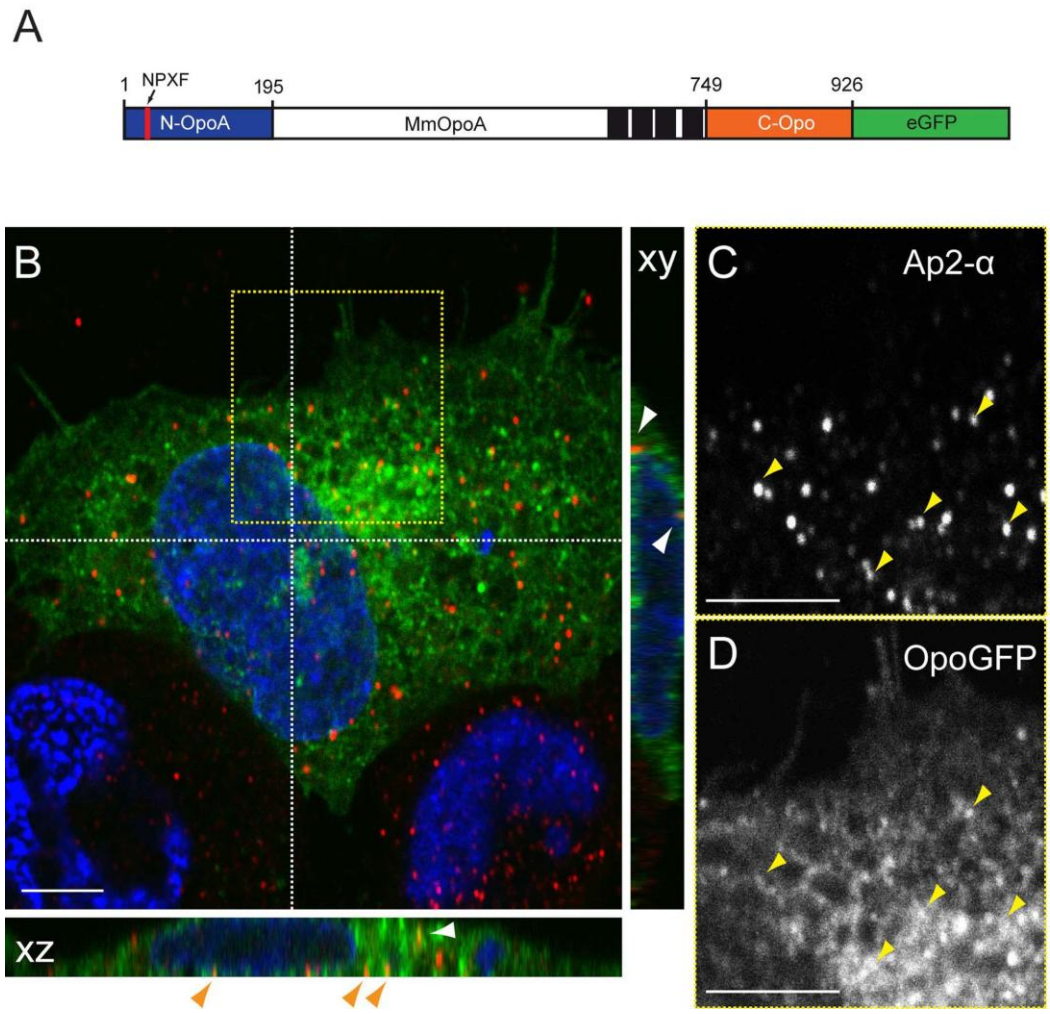

Figure S2. *Opo-GFP localizes to Ap2α-positive clathrin-coated structures (CCS).* (A-D) HeLa cells transfected with mouse Opo-GFP (A) were stained with anti- Ap2α antibodies to detect CCS. Colocalization (arrows) occurs preferentially at the cellular cortex (arrows in xz and xy projections) similarly to what was observed for the GFP-Opo fusion (see Figure 2). Bar= 5 µm

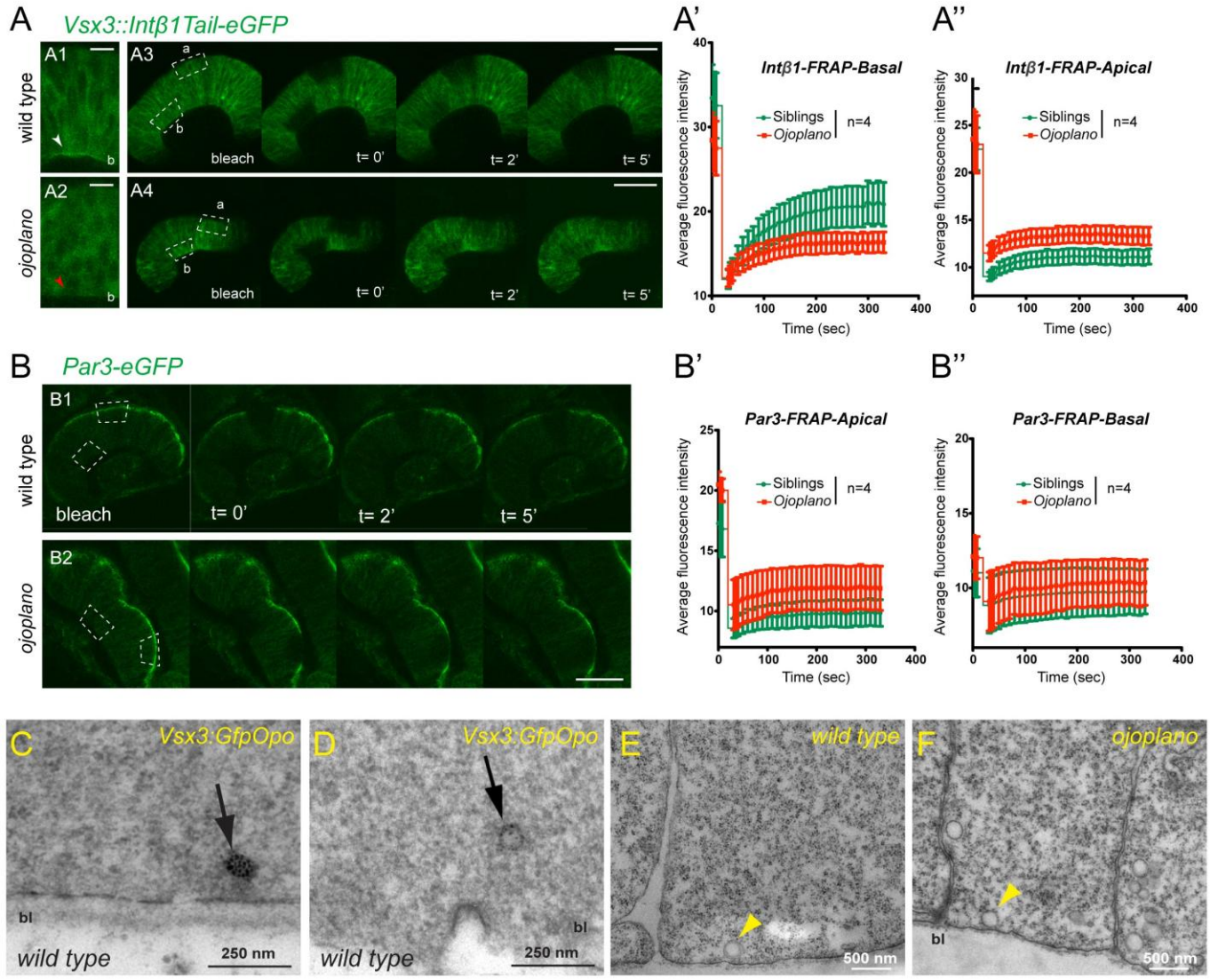

Figure S3. *FRAP experiments and EM analyses showing Opo function as a regulator of integrin trafficking.*

(A-B) *In vivo* FRAP reveals altered integrin-β1 trafficking in *opo* mutants**.**

(A1-A2) Confocal sections of stage 24 wt and *opo* mutant retinae showing Integrin-β1 distribution as visualized in the *Vsx3::Integrinβ1Tail-GFP* transgenic background. High magnification shows *Intβ1Tail-eGFP* accumulation at the basal side in wild type retinae, while being reduced in *opo*. (A3-A4) Transport dynamics of *Intβ1Tail-eGFP* were explored by FRAP. Equivalent areas were bleached from either basal or apical sides in stage 24 wild type (A3) and *opo* retinae (A4). Time points (in minutes) show Integrin recovery at the expenses of the unbleached half of the cells in wild type embryos. See also movies SM1 and SM2. (A'-A'') Average recovery curves (n=4) after basal (A') or apical (A'') FRAP plotted

for *opo* embryos (red) and their wild type siblings (green). Bar= 5 µm (A1, A2) 50µm (A3,A4).
(B-B'') As a control, the transport dynamics of *Par3-eGFP* was explored by FRAP in stage 24 wild type and *opo* retinae. Time points showing the tissue before and after photobleaching are indicated in minutes. The dotted lines mark bleached apical and basal areas. See also movies SM3 and SM4. Bar = 50 µm.

Note that the basal recovery of *Intβ1Tail-eGFP* (A') is reduced in *opo*, while the recovery of *Par3-eGFP* shows non-significant differences between wild type and mutants. It is important to state that the differential recovery between wild type and *opo* retinae occurs at the expenses of the unbleached region of the neuroblasts. In this 'donor' region there is no significant difference in fluorescence levels between wild type and *opo* embryos. Quantitative data are shown in Figure 4.

(C-F). *Electron microscopy analyses.*

(C,D) To examine the intracellular distribution of Opo in medaka neuroblasts, we performed immunogold labeling on ultra-thin sections from *Vsx3::eGFP_Opo* retinae at stage 23. Immunogold analysis revealed that Opo is associated to endosomes (arrows) at the basal end of the neuroepithelial precursors. eGFP_Opo was detected either after silver enhancement of ultra-small gold particles (C) or by directly visualizing the gold-conjugated secondary antibodies (D).

(E,F) EM analysis of stage 23 wild type (E) and *opo* (F) retinas reveals an accumulation of intracellular vesicles at the basal feet of the mutant neuroblasts. Vesicles (yellow arrows) were classified according to their size. Quantitative data are shown in Figure 4. Bar =500 nm.

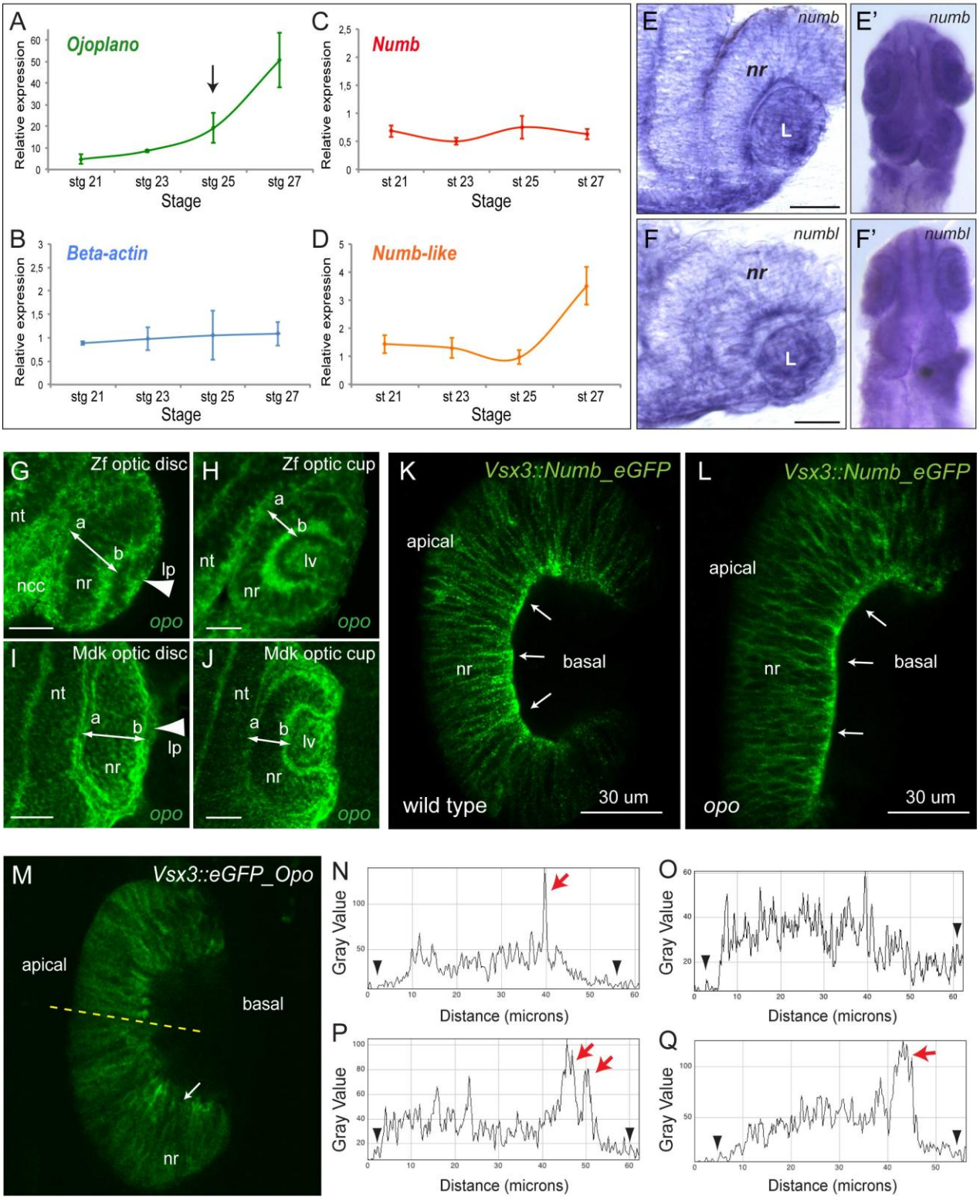
A
Ojoplano
Relative expression
stg 21
stg 23
stg 25
stg 27
Stage
B
Beta-actin
C
Numb
st 21
st 23
st 25
st 27
D
Numb-like
E
numb
nr
L
E'
F
numbl
F'
G
Zf optic disc
nt
a
b
lp
ncc
nr
opo
H
Zf optic cup
lv
I
Mdk optic disc
J
Mdk optic cup
K
Vsx3::Numb_eGFP
apical
basal
wild type
30 um
L
M
Vsx3::eGFP_Opo
N
Gray Value
Distance (microns)
O
P
Q

Figure S4**.** *numb, numbl and opo* expression in teleost embryos.
(A-F) *numb and numbl expression profiles in medaka embryos*.
(A-D) Relative expression levels of *opo* (A), control *beta-actin* (B), *numb* (C) and *numbl* (D) were analyzed by qPCR at four different developmental stages in medaka. The expression levels of *ef1* were used as an internal reference. Error bars in (A-D) represent SEM. Note that *opo* levels increase during optic cup folding stages (arrow). (E-F) Retinal sections of stage 24 medaka embryos hybridized with *numb* (E) and *numbl* (F) probes show that both transcripts are ubiquitously expressed through the tissue. *In toto* images are shown in E' and F' respectively. Bar= 50 µm.
(G-J) *Analysis of opo mRNA distribution by fluorescent in situ hybridization (FISH)*.
Confocal sections of zebrafish (G, H) and medaka (I, J) embryos show fluorescent labeling of *opo* transcripts during optic disc (G, I) and optic cup (H, J) stages. Note that *opo* transcripts are enriched at the basal side of the retinal epithelium in both species. lp= lens placode; lv= lens vesicle; ncc= neural crest cells; nr= neural retina; nt= neural tube; double arrows indicate the apico-basal (a-b) axis. Bar= 50 µm.
(K-L) *Numb_eGFP localization in mutant retinae.* Confocal sections show Numb_eGFP localization in wild type (K) and *opo* retinae (L) as visualized in the background of the *Vsx3::Numb_GFP* line *in vivo*. nr= neural retina. Bar= 30 µm.
(M-Q) *Quantification of Vsx3::eGFP_Opo signal through the retina*. Quantification of pixel intensity across a typical confocal image of a *Vsx3::eGFP_Opo* retina (M). Using Fiji's Plot Profile tool, pixel intensity was measured along the apico-basal axis. The lines were drawn in an apical-to-basal direction, and extending past the retinal tissue on either side of the epithelium, in order to measure background levels. (N-Q) Each plot corresponds to an individual measurement. Black arrowheads point to the line sections extending outside of the retina. Red arrows point to peaks of pixel intensity, which localize basally (6/8 cases analyzed; 4 are shown here). The analysis shows that *Vsx3:eGFP_Opo* is preferentially localized to the basal retina.

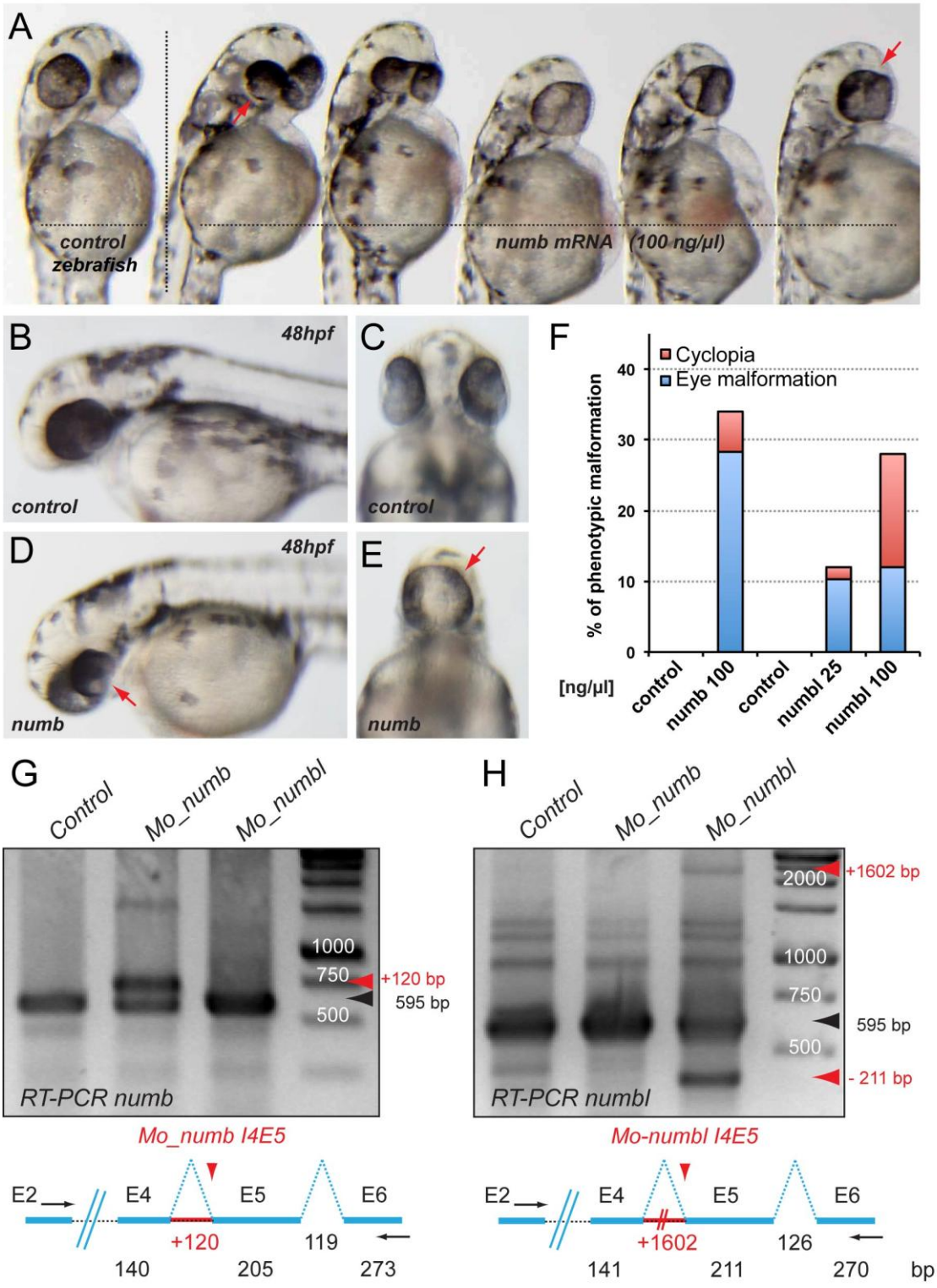
A
control zebrafish
numb mRNA (100 ng/µl)
B
48hpf
control
C
control
D
48hpf
numb
E
numb
F
Cyclopia
Eye malformation
% of phenotypic malformation
0
10
20
30
40
[ng/µl]
control
numb 100
control
numbl 25
numbl 100
G
Control
Mo_numb
Mo_numbl
1000
750
500
+120 bp
595 bp
RT-PCR numb
Mo_numb I4E5
E2
E4
E5
E6
+120
119
140
205
273
H
Control
Mo_numb
Mo_numbl
2000
1000
750
500
+1602 bp
595 bp
- 211 bp
RT-PCR numbl
Mo-numbl I4E5
E2
E4
E5
E6
+1602
126
141
211
270
bp

Figure S5. Genetic interaction *of opo* and numb/*numbl*.
(A-F) The injection of *numb* or *numbl* in zebrafish embryos results in severe ocular malformations. (A) 48 hpf control and treated zebrafish embryos injected with of *numb* RNA (100 ng/ µl) showing phenotypes ranging from flattened eyes to full cyclopia. Lateral (B, D) and ventral views (C, E) from control (B-C) and injected embryos (D-E) show ocular malformations such as: large ventral openings of the optic cup (D, arrow) and cyclopia (E, arrow). (F) Percentage of phenotypic malformations upon injection of increasing amounts of *numb* or *numbl* RNAs into zebrafish embryos.
(G-H) Co-injection of splicing morpholinos targeting *numb* and *numbl*. Specific splicing interferences caused by the morpholinos *Mo_numb_I4E5* (G) and *Mo_numbl_I4E5* (H) were monitored by RT-PCR in samples from control and morpholino-injected embryos. Relevant intron-exon structure and sizes (bp) as well as acceptors of splicing targeted by the morpholinos (red arrows) are depicted for each gene. Intron 4 read-throughs (G, H) and exon 5 skipping (H) are indicated in red. See also Figure 6.

Supplemental Movies

Movie SM1. *FRAP analysis of Intß1Tail-eGFP transport dynamics.*
Fluorescence recovery was analyzed in the retinae of stage 24 wild type (left) and *opo* (right) *Vsx3::Intß1Tail-eGFP* transgenic embryos. Equivalent areas in the retina were bleached either at the basal or the apical side of both wild type and *opo* retinae. A central optical section was recorded during 340 seconds (time resolution 10 s). See also Figure S3.

Movie SM2. *FRAP analysis of Par3-eGFP transport dynamics.*
Fluorescence recovery was analyzed in the retinae of stage 24 wild type (left) and *opo* (right) embryos injected with 50 ngr/µl of *Par3-eGFP*. Equivalent areas in the retina were bleached either at the basal or the apical side of both wild type and *opo* retinae. A central optical section was recorded during 340 seconds (time resolution 10 seconds). See also supplementary Figure S3.

Movie SM3. *In vivo localization of eGFP-Opo in the medaka retina during morphogenesis.*
Z-stack series of stage 24 *medaka retinae from the Vsx3::eGFP_Opo line.* Confocal images show *eGFP_Opo* enrichment at the basal (to the top) neuroblast feet. *A total of 24 images was collected and the distance between planes is 3 µm.* See also Figure 5.

Movie SM4. *In vivo localization of Numb-eGFP in the medaka retina during morphogenesis.*
Z-stack series of stage 24 medaka retinae from the *Vsx3::Numb-eGFP* line. Confocal images show *Numb-eGFP* enrichment at the basal (to the top) neuroblast feet. A total of 48 images was collected and the distance between planes is 2 µm. See also Figure 5.

Movie SM5. *Confocal time-lapse analysis of optic cup folding in wt and numbl-overexpressing embryos.*
Using the zebrafish *Vsx3::caaxGFP* line to monitor optic cup morphology, control (left) and *numbl* injected (right) 20hpf embryos were imaged in parallel using multiposition time-lapses for 3 hours with a time resolution of 3 min. Several central planes, spanning 40 µm, were selected for maximum projections. The injection of Lyn-tdTomato RNA as a control tracer had no effect on eye morphology. See also Figure 6.

Bogdanovic et al. Supplemental Table 1

(A) Y2H highest-scoring proteins for Opo N-terminal bait (Table S1A)

Screen = hgx2010v1 Vector = pB29 (N-OPO-LexA-C fusion)

Clone Name	PBS*	Gene Name (Best Match)	GID	%id 5p/3p	Start	Stop	Frame	Orientation
pB29_A-61	**B**	**Homolog of numbl (Danio rerio)**	GID: 190570255	97.8	na	1089	IF	Sense
pB29_A-38	**B**	**Homolog of numbl (Danio rerio)**	GID: 190570255	95.9 / 88.3	-1	1074	IF	Sense
pB29_A-79	**B**	**Homolog of numbl (Danio rerio)**	GID: 190570255	96.7 / 96.8	30	1090	IF	Sense
pB29_A-94	**B**	**Homolog of numbl (Danio rerio)**	GID: 190570255	99.8 / 99.7	30	1090	IF	Sense
pB29_A-49	**B**	**Homolog of numbl (Danio rerio)**	GID: 190570255	99.4	30	na	IF	Sense
pB29_A-83	**B**	**Homolog of numbl (Danio rerio)**	GID: 190570255	95.8	30	na	IF	Sense
pB29_A-16	**D**	**Homolog of DAB2 (Salmo salar)**	GID: 209151356	99.7 / 100	-1	1311	IF	Sense
pB29_A-36	**D**	**Homolog of grip1 (Danio rerio)**	GID: 113677822	99.0 / 99.4	-1	703	IF	Sense
pB29_A-13	**D**	**Homolog of IQ motif and Sec7 domain 2 isoform1, LOC560461 (Danio rerio)**	GID: 189522486	100	na	609	??	Sense
pB29_A-48	**D**	**Homolog of Khdrbs1 protein, BT027446 (Gasterosteus aculeatus);**	GID: 112420629	100 / 100	-1	913	IF	Sense
pB29_A-43	**D**	**Homolog of UPF0139 membrane protein C19orf56 cDNA (Tetraodon nigroviridis)**	GID: 56301860	100 / 100	-1	365	IF	Sense
pB29_A-5	**D**	**Homolog of Pias1, LOC564496 (Danio rerio)**	GID: 125821811	100 / 62.5	-1	na	IF	Sense
pB29_A-62	**D**	**Homolog of muscle-type creatine kinaseCKM1 (Oreochromis mossambicus)**	GID: 21694040	99.0 / 100	-1	1218	IF	Sense
pB29_A-23	**D**	**Homolog of Proteic Match - CXXC finger 1, like (D.rerio)**	GID: 41053355	100 / 57.7	-70	692	IF	Sense
pB29_A-11	**D**	**Homolog of PSMD2 (Salmo salar)**	GID: 223647425	100 / 100	-1	539	IF	Sense
pB29_A-26	**D**	**Homolog of LSM14a; zgc:77202 (Danio rerio);**	GID: 182890853	100 / 62.4	-1	na	IF	Sense

*Predicted Biological Score: Confidence for interactions. A= Very high, B= High, C= Good, D= Moderate

(B) Y2H highest-scoring proteins for Opo C-terminal bait (Table S1B)
Screen = hgx2010v2 Vector = pB27 (N-LexA-Opo-C fusion)

Clone Name	PBS*	Gene Name (Best Match)	GID	%id 5p/3p	Start	Stop	Frame	Orientation
pB27_A-39	A	Oryzias latipes - hspa1l	GID: 157278336	99.5 / 98.5	108	1475	IF	Sense
pB27_A-13	A	Oryzias latipes - hspa1l	GID: 157278336	99.5 / 98.5	474	1483	IF	Sense
pB27_A-38	A	Oryzias latipes - hspa1l	GID: 157278336	99.2 / 98.3	519	1473	IF	Sense
pB27_A-32	A	Oryzias latipes - hspa1l	GID: 157278336	98.3 / 98.3	762	1480	IF	Sense
pB27_A-41	A	Oryzias latipes - hspa1l	GID: 157278336	98.5 / 98.5	894	1480	IF	Sense
pB27_A-45	A	Oryzias latipes - hspa1l	GID: 157278336	97.6 / 97.6	1119	1482	IF	Sense
pB27_A-18	A	Oryzias latipes - hspa1l	GID: 157278336	97.6 / 97.6	1122	1491	IF	Sense
pB27_A-24	B	Homolog of Proteic Match - rapunzel 4 (D. rerio)	GID: 62955791	100 / 99.7	-64	891	IF	Sense
pB27_A-48	B	Homolog of Proteic Match - rapunzel 4 (D. rerio)	GID: 62955791	100 / 99.7	-64	891	IF	Sense
pB27_A-53	B	Homolog of Proteic Match - rapunzel 4 (D. rerio)	GID: 62955791	100 / 99.7	-64	891	IF	Sense
pB27_A-8	B	Homolog of Proteic Match - rapunzel 4 (D. rerio)	GID: 62955791	99.6 / 99.7	-58	888	IF	Sense
pB27_A-11	B	Homolog of Tnks (Rattus norvegicus)	GID: 157821502	98.5 / 63.6	-1	930	IF	Sense
pB27_A-14	B	Homolog of Tnks (Rattus norvegicus)	GID: 157821502	99.8 / 63.6	-1	930	IF	Sense
pB27_A-25	B	Homolog of Tnks (Rattus norvegicus)	GID: 157821502	100/ 96.7	501	1379	IF	Sense
pB27_A-44	B	Homolog of Tnks (Rattus norvegicus)	GID: 157821502	99.8 / 99.3	-1	1363	IF	Sense
pB27_A-6	B	Homolog of Tnks (Rattus norvegicus)	GID: 157821502	99.2 / 99.7	426	1349	IF	Sense
pB27_A-10	C	Homolog of LOC567533 (D. rerio); D. rerio novel protein similar to vertebrate tankyrase	GID: 190339365	99.9 / 99.8	-1	1294	IF	Sense
pB27_A-29	C	Homolog of LOC567533 (D. rerio); D. rerio novel protein similar to vertebrate tankyrase	GID: 190339365	99.3 / 99.5	195	1411	IF	Sense
pB27_A-34	C	Homolog of RING1 BT028051 (G. aculeatus)	GID: 112421314	96.4 / 98.5	-1	817	IF	Sense
pB27_A-46	C	Homolog of RING1 BT028051 (G. aculeatus)	GID: 112421314	99.8 / 84.1	72	1281	IF	Sense
pB27_A-30	D	Homolog of GFPT1 (Salmo salar)	GID: 209155159	99.9 / 93.0	-1	1093	IF	Sense
pB27_A-36	D	Homolog of GFPT1 (Salmo salar)	GID: 209155159	99.7 / 99.5	-1	1093	IF	Sense
pB27_A-31	D	Homolog of Gmeb2 (Mus musculus)	GID: 118130813	100/ 94.8	-1	817	IF	Sense
pB27_A-15	D	Homolog of Grp78 (Paralichthys olivaceus)	GID: 110226519	99.1 / 99.8	-1	971	IF	Sense
pB27_A-43	D	Homolog of metabotropic glutamate receptor 8-likeLOC569768 (Danio rerio)	GID: 189537612	100/ 100	-1	452	IF	Sense
pB27_A-40	D	Homolog of Proteic Match - PREDICTED: alpha-2 macroglobulin like-protein (Danio rerio)	GID: 189528666	99.8 / 100	-1	878	IF	Sense
pB27_A-47	D	Homolog of Proteic Match - PREDICTED: alpha-2 macroglobulin like-protein (Danio rerio)	GID: 189528666	100 / 99.7	-1	878	IF	Sense
pB27_A-33	D	O. latipes HS 70kDa prot 2 isoform mRNA	GID: 146160709	100 / 99.5	285	1239	IF	Sense

*Predicted Biological Score: Confidence for interactions. A= Very high, B= High, C= Good, D= Moderate

Table S1. List of Y2H highest-scoring proteins for Opo N-terminal bait (Table S1A) and C-terminal bait (Table S1B).

Bogdanovic et al. Supplemental Table 2

Opo and numb/numbl genetic interaction

A) *Numbl* mRNA injection (25 ng) in embryos from wild type (iCAb) and *opo* carriers.

	Experiment 1				**Experiment 2**				**Experiment 3**			
Phenotype /Treatment	iCab /Ctrl	iCab /25 ng	*opo* /Ctrl	*opo* /25 ng	iCab /Ctrl	iCab /25 ng	*opo* /Ctrl	*opo* /25 ng	iCab /Ctrl	iCab /25 ng	*opo* /Ctrl	*opo* /25 ng
Total(Survival 48hpf)	45	31	324	36	53	41	99	48	42	30	25	18
Wild type phenotype	45 100%	27 87.1%	247 76.2%	19 52.8%	53 100%	37 90.2%	75 75.8%	26 54.2%	42 100%	26 86.7%	19 76%	10 55.5%
Optic cup malformation	0 0%	4 12.9%	77 23.8%	17 47.2%	0 0%	4 9.8%	24 24.2%	22 45.8%	0 0%	4 13.3%	6 24%	8 44.5%
Cyclopia	0 0%	0 0%	0 0%	2 5.6%	0 0%	0 0%	0 0%	2 4.2%	0 0%	0 0%	0 0%	0 0%

B) Co-injection of *Mo_Numb* (50 µM) and *Mo_numbl* (100µM) in embryos from wild type (iCAb) and *opo* carriers.

	Experiment1				**Experiment2**				**Experiment3**			**Experiment4**	
phenotype /treatment	iCab /Ctrl	iCab /Mo	*opo* /Ctrl	*opo* /Mo	iCab /Ctrl	iCab /Mo	*opo* /Ctrl	*opo* /Mo	iCab /Ctrl	*opo* /Ctrl	*opo* /Mo	iCab /Ctrl	*opo* /Ctrl
Embryos scored	41	29	42	53	83	35	61	22	61	47	83	52	49
Wild type phenotype %	100 %	100 %	71,4 %	69,8 %	100 %	100 %	77,1 %	77,3 %	100 %	76,6 %	72,3 %	100 %	73,5 %
***Opo* phenotype %**	0 %	0 %	28,6 %	18,9 %	0 %	0 %	22,9 %	9,10 %	0 %	23,4 %	16,9 %	0 %	26,5 %
Rescued %	0 %	0 %	0 %	11,3 %	0 %	0 %	0 %	13,6 %	0 %	0 %	10,8 %	0 %	0 %

Table S2. Genetic interaction *of opo* and numb/*numbl*.
A) *numbl* mRNA injection in embryos from wild type (iCAb) and *opo* carriers. The table includes raw data from three different experiments showing the distribution of eye phenotypes in medaka embryos injected either with *numbl* RNA (25 ng/µl) or mock-treated (Ctrl), both in a wild type (iCAb) or mutant *opo* (*opo*) background.
B) Co-injection of *Mo_numb* and *Mo_numbl* in embryos from wild type (iCAb) and *opo* carriers. The table includes raw data from three independent experiments and shows the distribution of eye phenotypes in medaka embryos co-injected with *Mo_numb* (50 µM) and *Mo_numbl* (100 µM) or mock-treated (Ctrl), both in a wild type (iCAb) or mutant (*opo*) background.

Supplemental Experimental Procedures.

Fish stocks: Both medaka (*Oryzias latipes*) Cab (wild-type) and *Ojoplano* lines as well as Zebrafish (Danio rerio) of the WIK/AB wild-type strain were kept in closed stocks at the CABD. Embryos were staged as described (Iwamatsu, 2004; Kimmel et al., 1995).

Expression constructs: The following vectors were used in pull-down and IP experiments: The medaka *ojoplano* vectors: *pCS2+:opo* (including the full-length *opo* cDNA under the control of a CMV promoter) and *pGEX-Kg:opo_N* (engineered to fuse the 112 aa N terminal fragment of the protein to GST) were previously described (Martinez-Morales et al., 2009). The medaka *Dab2* full-length clone *FOE002-P00108-DPE-F_J11* (GeneBank: AM334754) was derived from an unigene library (Souren et al., 2009) and cloned into pCS2+ (*pCS2+:Dab2*). The amino fragment of this clone, encoding the 210 N-terminal aa of Dab2, was cloned in pCS2+ (*pCS2+:N-Dab2*) and fused to the *GST* C-terminus (pGEX-KG:*N-Dab2*). The medaka *numb* full-length clone *FOE002-P00118-DPE-F_E03* (GeneBank: AM338138) was cloned into pCS2+ (*pCS2+:Numb*). The amino fragment of this clone, encoding the 219 N-terminal aa of Numb, was cloned in pCS2+ (*pCS2+:N-Numb*) and fused to the *GST* C-terminus (*pGEX-KG:N-Numb*). The medaka *Numbl* full-length clone, homologous to the cDNA clone olec7n19 (GeneBank: DK138204.1), was derived from the Y2H library and cloned into pCS2+ (*pCS2+:Numbl*). The amino fragment of this clone, encoding for the 214 n-terminal aa of Numbl, was cloned in pCS2+ (*pCS2+:N-Numbl*) and fused to the C-terminus of *GST* (*pGEX-KG:N-Numbl*) or (6x)Myc tag (*pCS2+:Myc-N-Numbl*). The following vectors were used in colocalization experiments: The mouse *ojoplano* fusions *OpoA_GFP*, *GFP_OpoA* and *GFP_OpoB* cloned into *pEGFP* vectors, were previously described (Mertes et al., 2009). The carboxy-terminal truncation of *GFP_OpoA* was generated by removing the sequence coding for the last 132 aminoacids of the protein.The fusion zNumb:Cherry (*pCS2+:zNumb:Cherry*) was obtained by replacing the GFP sequence by Cherry in the construct z*Numb(PTBL PRRL):*eGFP (Reugels et al., 2006).

Immunogold studies: *Vsx3::eGFP_Opo* embryos were fixed in 0.1 M sodium cacodylate buffer, pH 7.3, containing 4% paraformaldehyde and 0.25% glutaraldehyde for 2 hours at 4 °C. Samples were washed in cacodylate buffer, blocked in 4% bovine serum albumin (BSA), 0.5% Tween20 in PBS, pH 7.4, for 2 h at 4 °C and incubated with rabbit polyclonal anti-GFP antibody (A-11122, Invitrogen) diluted 1:100 in blocking solution with 0.02% NaN_3 for 48 h at 4 °C. After washes with PBS, samples were then incubated with ultra-small gold-conjugated goat anti-rabbit secondary antibody (Aurion, NL) diluted 1:50 in 4% BSA, 0.5% Tween20 and 0.02% NaN_3 in PBS. After washes, gold particles were silver enhanced with R-gent SE-EM (Aurion, NL) at RT for 30 min, washed and post- fixed with 2% glutaraldehyde in PB for 20 min at 4 °C. Finally, samples were fixed with 0.5% osmium tetroxide for 20 min at 4 °C, dehydrated, and embedded in EMbed 812 resin (14120, EMS). Ultra-thin sections, stained with lead citrate (Leica) and uranyl acetate (Merck), were examined under a Philips CM 120 BioTwin or a Zeiss EM900 electron microscope (120 kV).

qPCR: Total RNA was extracted from medaka embryos at the developmental stages indicated (18 to 27). Then, cDNAs were synthesized with SuperScript VILO cDNA synthesis kit (Invitrogene). The qRT-PCR was performed using the SsoFast Evagreen supermix (Biorad) according to the manufacturer's instructions in a CFX96 real-time C1000 thermal cycler

(Biorad). The expression levels of *numbl*, *numb* , *ojoplano*, *ef-1* and *β-actin* were measured using the BioRad CFX Manager software. The following primers were employed:
numbl 5'-GGCAGAGTCTGAGGAGGAAGAA-3'; 5'-CTCCTCACAGACGTGCATCCCT-3',
numb 5'- TCAGCCAGAAGACGTCGCCGT -3'; 5'- CTGAAGGTGGTGGTGATCTGG-3',
ojoplano 5'- TTTCCCTCTTTAGCGGTGAGT-3'; 5'- CGGGTGCAGCAGGAGTGTTC -3',
ef-1 5'- AAACCCAGAAACACCGAAACA -3'; 5'- CCTCCGCACTTGTAGATCAG -3',
β-actin 5'- CAACAGGGAGAAGATGACC -3'; 5'-CCAGAGTCCATGACGATACCA-3'.

The efficiency of the primers and the relative quantification were calculated using a previously described mathematical model (Pfaffl, 2001).

***WISH*:** Whole-mount in situ hybridization was performed using digoxigenin labeled riboprobes as described (Martinez-Morales et al., 2005). For vibratome sections embryos were embedded in the gelatin/albumin and sectioned at 30 μm thick (Leica).

***Fluorescent in situ hybridization (FISH)*:** FISH was performed according to standard protocol (Lauter et al., 2011). Briefly, dechorionated medaka and zebrafish embryos were fixed in 4% paraformaldehyde overnight at 4°C, dehydrated in methanol series, then rehydrated and treated with 20 μg/ml proteinase K (Sigma) for 8 minutes. Digoxigenin-labelled probes were hybridized overnight at 68°C and detected using anti-digoxigenin-POD antibody *(nº cat. 11426346910, Roche Applied Science)* at 1:2000 dilution. The embryos were then incubated with tyramide-FICT at a dilution 1:100 (*TSA systems, PerkinElmer*), and treated with H_2O_2 at 0,001% followed by H_2O_2 at 1% to stop the reaction. Embryos were analyzed using a *Leica SPE* confocal system.

Morpholino injections: Rescue experiments were performed by injecting medaka embryos with splicing morpholinos obtained from Gene Tools. The following morpholinos were injected:

Mo_numb-I4E5: 5'- TCCCCCTGAAACAAACCACCCACAC-3'. (50 μM).

Mo_numbl-I4E5: 5'- CTCCCCCTGGAGCCGGAGAAGAACC-3' (100 μM).

Splicing interference events were monitored by RT-PCR in samples from wild type and morpholino injected embryos. To this end, total RNA was extracted from each sample (TRIzol, Invitrogen) and RT reactions were performed (Super Script III, Invitrogen). The following primers were used in RT-PCR experiments:

Ctrl_Mo_numb_fw: 5'- CAGCTTCGCAGTCAAGTACCTGG- 3'

Ctrl_Mo_numb_rv: 5'- AGGGGTTCGTCACACAGTTTGCAG- 3'

Ctrl_Mo_numbl_fw: 5'- GCAGACCGCATCAGTGGCAGGCAG- 3'

Ctrl_Mo_numbl_rv: 5'- GGTGGAAGGGCGGGAACAACACAG- 3'

Confocal time lapse analyses: Control and injected 20hpf *Vsx3::caaxGFP* embryos were immobilized in E3 (containing 0.01% tricaine) and embedded in 1% low-melting agarose. Time-lapse analyses were performed on a Nikon A1R microscope with a CFI PlanFluor20xMI N.A.0.75 objective and a 488 nm laser line. Samples were imaged as multiposition time-lapses for 3 hours with a time resolution of 3 min. Several central planes, spanning 40 μm, were selected. Movies were put together with single planes from each Z-stack using ImageJ (NIH).

Supplemental References

Iwamatsu, T. (2004). Stages of normal development in the medaka Oryzias latipes. Mech Dev *121*, 605-618.

Kimmel, C.B., Ballard, W.W., Kimmel, S.R., Ullmann, B., and Schilling, T.F. (1995). Stages of embryonic development of the zebrafish. Dev Dyn *203*, 253-310.

Lauter, G., Soll, I., and Hauptmann, G. (2011). Two-color fluorescent in situ hybridization in the embryonic zebrafish brain using differential detection systems. BMC Dev Biol *11*, 43.

Martinez-Morales, J.R., Del Bene, F., Nica, G., Hammerschmidt, M., Bovolenta, P., and Wittbrodt, J. (2005). Differentiation of the vertebrate retina is coordinated by an FGF signaling center. Dev Cell *8*, 565-574.

Martinez-Morales, J.R., Rembold, M., Greger, K., Simpson, J.C., Brown, K.E., Quiring, R., Pepperkok, R., Martin-Bermudo, M.D., Himmelbauer, H., and Wittbrodt, J. (2009). ojoplano-mediated basal constriction is essential for optic cup morphogenesis. Development *136*, 2165-2175.

Mertes, F., Martinez-Morales, J.R., Nolden, T., Sporle, R., Wittbrodt, J., Lehrach, H., and Himmelbauer, H. (2009). Cloning of mouse ojoplano, a reticular cytoplasmic protein expressed during embryonic development. Gene Expr Patterns *9*, 562-567.

Pfaffl, M.W. (2001). A new mathematical model for relative quantification in real-time RT-PCR. Nucleic Acids Res *29*, e45.

Reugels, A.M., Boggetti, B., Scheer, N., and Campos-Ortega, J.A. (2006). Asymmetric localization of Numb:EGFP in dividing neuroepithelial cells during neurulation in Danio rerio. Dev Dyn *235*, 934-948.

Souren, M., Martinez-Morales, J.R., Makri, P., Wittbrodt, B., and Wittbrodt, J. (2009). A global survey identifies novel upstream components of the Ath5 neurogenic network. Genome Biol *10*, R92.